論文 / 著書情報
Article / Book Information

題目(和文)	
Title(English)	Evaluation method of photoacoustic contrast agent
著者(和文)	ZengXi
Author(English)	Xi Zeng
出典(和文)	学位:博士(工学), 学位授与機関:東京工業大学, 報告番号:甲第10708号, 授与年月日:2017年12月31日, 学位の種別:課程博士, 審査員:中村 健太郎,小池 康晴,黒澤 実,杉野 暢彦,和田 裕之
Citation(English)	Degree:Doctor (Engineering), Conferring organization: Tokyo Institute of Technology, Report number:甲第10708号, Conferred date:2017/12/31, Degree Type:Course doctor, Examiner:,,,,
学位種別(和文)	博士論文
Type(English)	Doctoral Thesis

Evaluation method of photoacoustic contrast agent

Tokyo Institute of Technology

Xi Zeng

Evaluation method of photoacoustic contrast agent

A DISSERTATION SUBMITTED IN PARTIAL
FULFILLMENT OF THE REQUIREMENTS

for the degree

DOCTOR OF ENGINEERING

Supervisor: **Professor Kentaro NAKAMURA**

指導教員:　中村 健太郎　教授

Department of Information Processing
Interdisciplinary Graduate School of Science and Engineering
Tokyo Institute of Technology

By

Xi Zeng
曾 晞

September 2017

Abstract

Noninvasive imaging and sensing technology for health diagnosis and biomedicine research is one of the most stimulating fields. There are several conventional methods available, such as X-ray, magnetic resonance imaging, ultrasound and optical methods (microscopy or optical coherence tomography). But these have limitations in imaging depth or spatial resolution or cost. Photoacoustics is a promising solution combining optical and acoustics techniques and has a possibility to overcome some of the limitations with conventional methods. Photoacoustic tomography could provide good detecting depth with higher resolution and contrast. It is a suitable method for opaque and solids, especially for biological structures. Photoacoustics has been applied in different fields in the past 30 years, including material science, gas analysis, and biomedicine. Number of paper publication related to photoacoustics has been increasing for this decade. Among them, medical application of photoacoustic tomography is rapidly expanding. In the first generation of photoacoustic imaging, it adopts human elements as target absorber. Recently, second generation adopting high-absorption contrast agent is becoming hot topic since it has a possibility to extend the application from genetic to whole human body imaging. Thus, it is important to shorten the development period of highly efficient contrast agent. These backgrounds of this study is described in Chapter 1.

To meet the demand, in Chapter 2, we have proposed a compact and cost-effective evaluation system for photoacoustic contrast agents for biomedicine application. This system adopts dual laser diodes at different wavelengths (660 and 785 nm) working with modulated continuous waves and a small microphone of low-frequency (kHz) region. As preliminary measurement, the characteristics of the photoacoustic system are experimentally invested for ink solutions (black ink and dye ink) and their mixture. The proposed system could distinguish a 10-mg/dl concentration difference of the black ink solution and the mixture ratio of black and dye ink. It was also possible to discriminate a

small absorption difference of water at the wavelengths of 660 and 785 nm.

In Chapter 3, some of known contrast agents were tested using this photoacoustic system to confirm its effectiveness and sensitivity as a standard evaluation system. It was succeeded to distinguish 2.5 mg/dl of the concentration difference of ICG solution. It was proved that the proposed method could be applied for sample with small volume, and could be used for liquid, solid and powder testing. Moreover, the high sensitivity and characteristics of this PA evaluation system have been demonstrated in this thesis.

Beside the photoacoustic evaluation system, a novel acoustic detector array was proposed and investigated in Chapter 4, with thinking future application for photoacoustic imaging. Piezoelectric ceramic (PZT) transducer has been used for conventional acoustic detector and its array has problem with metal wire bundle, which are heavy, large and short in transmitting distance. Here, we propose a new acoustic detector, called 'LED-PZT sensor array,' which consists of light emitting diode (LED) and PZT element, and its output signals are transmitted through a plastic optical fiber. Preliminary measurements using a single LED-PZT sensor were demonstrated for 26-kHz, 38-kHz and 1.6-MHz ultrasound fields underwater, respectively. Then, the sensor array with four LED-PZT sensors were utilized to measure sound pressure distribution in the 26-kHz ultrasonic field in water and demonstrated its effectiveness by comparing the results with a conventional hydrophone. Sound intensity is an important vector quantity in acoustics and capable to provide both magnitude and direction of the energy flow by sound waves. We use four LED-PZT sensors, called sound intensity probe, to measure sound intensity distribution in 26-kHz ultrasonic field in water. Differences were successfully observed in the sound intensity maps between with and without absorbers on the walls of water tank. It has no limitation to extend cable length of sensor and no concern with the weight of cable (33% of conventional hydrophone weight). A possible configuration for large scale arrayed detector utilizing wavelength division multiplexing technique was discussed.

In Chapter 5, summaries of this study and future work were presented.

Acknowledgements

This thesis would not have been possible without the help and support of a number of people. The individual I am most indebted to is my supervisor, Prof. Kentaro Nakamura. It is my honor to be his student. He provided me such an exciting and promising research topic, which aroused my interest and curiosity. In the past three years, when meeting research problems, I always could get supports and inspirations from him, although he was always very busy. His wisdom and patience not only taught me knowledge, but also taught me how to think and how to analyze. My methodology techniques and comprehensive research ability have been polished off by these discussions day by day. I have years' working experiences in industry before coming here and know how precious it is to have opportunity to consult a master like him, which are invaluable to me. Beside academy, Prof. Kentaro Nakamura also showed me how to get along and communicate with different people. He provide a permissive environment in our laboratory for students to enjoy the balance of life and research. All of our students respect him and feel lucky to be a member in his laboratory, including me.

I also express my appreciation to the members of my thesis committee, Prof. Minoru Kurosawa, Prof. Nobuhiko Sugino, Prof. Hiroyuki Wada, Prof. Yasuharu Koike. Thanks for their inspiring advices and challenging questions. I have learned a lot from those valuable discussions.

I am grateful to Asst. Prof. Yosuke Mizuno and Mrs. Mayumi Azuma in our Nakamura laboratory. Mrs. Mayumi Azuma friendly helped me to handle some daily life problems and prepare documents in Japanese. And I also want to say thank to other students in our laboratory for their support and the happy time we enjoyed together.

As for the experiments of photoacoustic contrast agents, I would like to express my appreciation to Prof. Shinichiro Fuse and Prof. Hiroyuki Nakamura for preparing the contrast agent samples and fruitful discussions of experimental results. These discussions

and tests help to deepen my understanding with my photoacoustic system and the characteristics of contrast agents.

Moreover, I really thanks Goenkaji and Praveenji, who lovingly taught me important things.

Finally, I want to dedicate this work to my father and my mother. After my years' working experiences, they still unconditionally understand and support me to back to university to try new life and explore new world. Their grace and calmness give me another lesson of life.

Contents

Chapter 1
Introduction

1.1 Conventional medical imaging techniques

Non-invasive imaging and sensing technology for health diagnosis and biomedicine is one of the most stimulating fields now. X-ray CT, Ultrasonography, MRI and optical method are the most common non-invasive medical imaging in hospital [1]. Normally we use these parameters to characterize different imaging tools, such as contrast, spatial resolution, imaging depth, safety, cost, speed of data acquisition. These conventional methods have their limitation in some parameters.

Table 1.1 shows conventional medical imaging methods [1] [2]. X-ray CT can provide good resolution (100 μm) and full-body imaging depth, but has risk of ionizing. MRI is a great tool which can provide great contrast, resolution (25-100 μm), full-body imaging depth and rich function. However, it is slow to get data and the cost is high. Ultrasonography has good imaging depth (300 mm) and resolution (30 μm), but unfortunately, the contrast is bad comparing with optical method. It leads to unclear images. While optical imaging, including microscopy and OCT (optical coherence tomography), have great contrast and resolution (0.5-10 μm), however, the imaging depth is poor. Comprehensively, if we have a method combining the advantages of ultrasound and optics, it will be a wonderful choice for imaging and sensing.

Table 1.1 conventional medical imaging.

Characteristics	X-ray CT	MRI	Ultrasound	Optical imaging (OCT, Microscopy)
Soft-tissue contrast	Poor	Excellent	Poor	Excellent
Spatial resolution (um)	100	25-100	30	0.5--10
Imaging depth (mm)	Full body	Full body	300	0.2--2
Safety	No	Yes	Yes	Yes
Data acquisition	Slow	Slow	Fast	Fast
Cost	High	High	Low	Low

Photoacoustic (PA) method provide such solution to meet this demand, by combining optical and acoustic waves, giving an excellent method for non-invasive imaging and sensing. Photoacoustic imaging has appropriate contrast, spatial resolution and depth of imaging [3].

1.2 Photoacoustic system

1.2.1 Working principle and features of photoacoustics

Photoacoustic (PA) method mainly consists of two parts: optical excitation and acoustic detection. Fig. 1.1 show the working principle of photoacoustic method. Firstly, we use a light to irradiate the measured target. The common light source is laser due to its high power density, and LED is possible too. Then the target absorbs the photons and convert it into heat. Temperature rises and thermoelastic expansion happens. The acoustic signals

are launched by thermally-induced pressure jump. Finally, we use transducer or microphone to detect the acoustic waves (called photoacoustic waves too) to form imaging or sensing results. Fig. 1.2 shows the fundamental process of PA method. Photoacoustic signal (PAS) is proportional to the optical power and the absorption coefficient of measurement target.

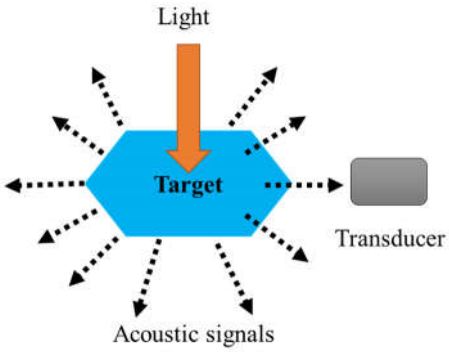

Fig. 1.1 Working principle of photoacoustics

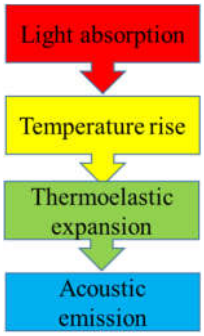

Fig. 1.2 Fundamental process of PA method.

Fig. 1.3 shows the comparison between optical, ultrasound and photoacoustic methods. Current optical methods, microscopy and OCT, can provide excellent resolution. However, the imaging depth is poor and can only reach skin level of human tissue. While

the imaging depth of ultrasound is very good, covering from cell to organ level, but the resolution is poor, which makes the imaging is not clear. PA method combines optics and acoustics to bridge the gap of imaging depth between organelle and organ, and at the same time keeps the high resolution.

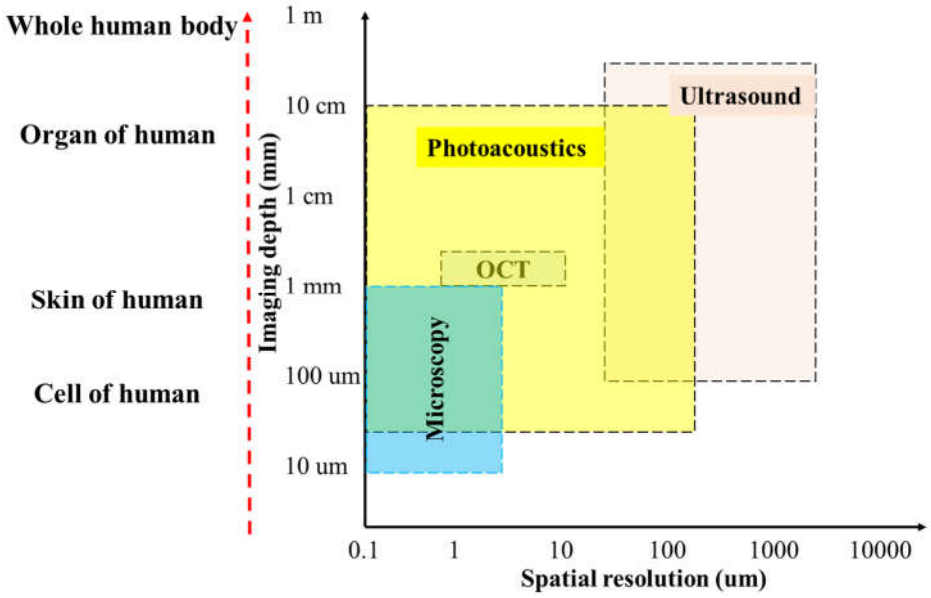

Fig. 1.3 Comparison of optical, ultrasound and photoacoustic method.

PA method combines optical and acoustic waves, which bring several advantages [4]: (1) PA method provides deeper penetration comparing with pure optical methods, because acoustic scattering is only 1/1000 of optical scattering. (2) Multicontrast and multiscale imaging are available with high resolution of living biological structure. (3) It is suitable method for opaque and solids, especially for biological structures. (4) It can provides selective sensitivity by choosing an appropriate light source. (5) It can adopts contrast agent to revolutionize the biomedical diagnosis and treatment.

In history, there are two main challenges of optical methods, including photoacoustics. The first challenge is spatial resolution of optical system. The fundamental minimum of spatial resolution of microscope is limited by the optical diffraction in theory. Diffraction limit the spatial resolution to half of the wavelength in the medium [5]. Equation (1.1) and fig. 1.4 show the resolution limit of the microscope. d is the minimum size could be observed by microscope; α is the angle of converging light; λ_n is the optical wavelength in medium with refractive index n. When α is π/2, d is minimum and is half wavelength in the medium.

$$d = \frac{\lambda_n}{2\sin\alpha} \tag{1.1}$$

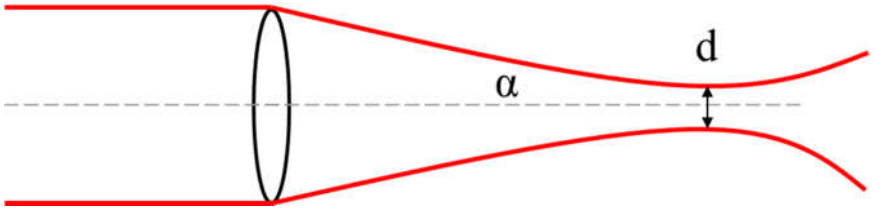

Fig. 1.4 the minimum resolution of the microscope.

The second challenge for optical method is penetration depth presenting more difficulties due to optical scattering and absorption. In the past 350 years, human developed different optical tools to conquer penetration limitation: microscopy (penetration depth: 100 μm, cell level penetration), confocal microscopy and OCT (penetration depth: 1 mm, skin level,), and recently photoacoustics (penetration depth: 10 cm, organ level). Comparing with conventional optical methods, photoacoustics is the first optical tool providing imaging and sensing information of living biological structures

for such wide penetration range: from organelles to organs [6]. By adopting contrast agent, PAT may provide the images of full human body.

Biomedicine is the major application of photoacoustics. When irradiating biological tissue, the light will be attenuated by scattering and absorption. Scattering coefficient has a representative value of 100 cm^{-1} in biological tissue, while absorption coefficient is 0.1 cm^{-1} in biological tissue. It means the optical scattering of tissue is 1000 times of optical absorption and light is mainly attenuated by scattering. Moreover, the cell is the basic unit of plant and creature, and its size is 1-100 μm. Optical scattering in these cells can be modeled by the Mie theory and is independent of optical wavelength. So when choosing light source wavelength for biological tissue measurement, we just need to consider the effect of optical absorption rather than scattering. As for the safety of electromagnetic wave, when the wavelength reduces to X-RAY or gamma, the radiation will damage DNA of creature and it is not safe to use. Normally, we will adopt wavelength from about 400 nm to 1 mm as light source of photoacoustic method.

1.2.2 History and development of photoacoustics

In 1880, Alexander Graham Bell found first photoacoustic phenomenon [7]. He adjusted the sunlight to irradiate a cell. Then he used a telephone receiver to hear the acoustic signal and found the acoustic signals changed according to the sunlight.

Modern PA research started from 1975 thanks to the development of high-performance light source and acoustic detector. In 1976, the famous Rosencwaig–Gersho theory was proposed and provided the theoretical foundation of PA spectroscopy on solid samples. Since then, PA have been applied in different fields and numerous PA systems

have been developed to test liquid-, solid-, and gas-phase non-destructively [8], for example material science, liquid or gas analysis [9], and biomedicine [10] etc.

In order to analyze the development of photoacoustics and get the whole picture of this research, we have searched the keywords of photoacoustics in the website of Web of Science and used software Histcite to analyze the published papers in photoacoustics field in the past several decades. Table 1.2 shows the current main features of photoacoustics. Approximately, photoacoustic research, as a non-destructive method, could be divided into four different fields according to research target.

The biggest PA research field is photoacoustic tomography (PAT) to provide imaging for biomedical application [11-13]. Approximately, 50% of published paper in photoacoustics come from this field. Human tissue is the main target. This research started from around 1975 and has been rapidly developed since 2005 [14]. Around half of published papers in photoacoustics come from this field. Imaging of brain activity and structure is hot topic in this field [15-16]. Moreover, quantitative PA imaging rather than qualitative analysis is also important, for example hemoglobin oxygen saturation in the image [17-18]. There are three major implementations now of PAT [3]: focused-scanning photoacoustic microscopy (PAM) [19-20], photoacoustic computed tomography (PACT) [21], and photoacoustic endoscopy (PAE) [22]. Fig. 1.3-1.5 show the confirgureation of PAM, PACT and PAE. PAM and PAE could provide resolution with micrometer scale at millimeters imaging depth, while PACT could provide image with microscopic and macroscopic scale. Every implementation could be classified into diverse prototype according to the specific application demands, and the laser source and transducer change correspondingly. Another technical trend is to develop PAT system based on a clinical matrix array ultrasound probe [23-24]. The equipment of PAT are large and expensive.

Because it normally adopts nanosecond-pulsed laser as light source and megahertz ultrasonic transducer as detection. Moreover, imaging processing system is necessary too [25], and mechanical system to move light source or transducer array may also needed for scanning the measurement target.

Table 1.2 Categories of photoacoustic research.

Categories	**PAT (biomedical imaging)**	**Gas and aerosols analysis**	**Process analysis**	**Photoacoustic theory**
Ranking	Biggest field ~ 50%	Second biggest ~ 25%	Small filed ~ 15%	Small filed ~ 10%
Main contents	Imaging of biomedicine	Gas tracing; Quantitative Measurement;	Characterization of materials;	Light-acoustics, light-heat transforming;
Main target	Human tissue	Gas and aerosols	Solid, semisolid and liquid	All kinds
Main development period	2005-present	1995-2010	1975-2000	1985-2000
Key words	photoacoustic imaging, tomography	Photoacoustic spectroscopy, gas and aerosols tracing;	Photoacoustic spectroscopy, measurement;	Photoacoustic, photothermal theory
Hot spot and new trend	Brain activity and structure; Quantitative measurement of imaging;	Quantum cascade lasers for gas trace; Agricultural applications; Food packaging;	Biomedicine measurement;	No

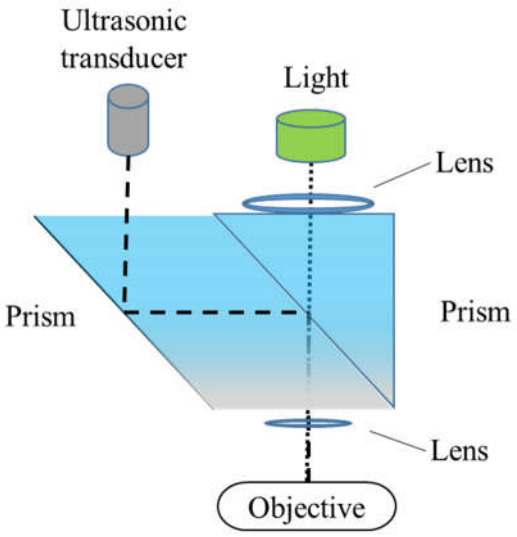

Fig. 1.3 Focused-scanning photoacoustic microscopy (PAM).

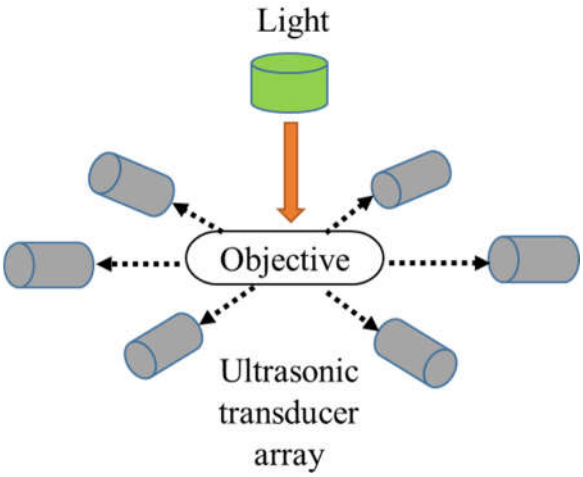

Fig. 1.4 Photoacoustic computed tomography (PACT)

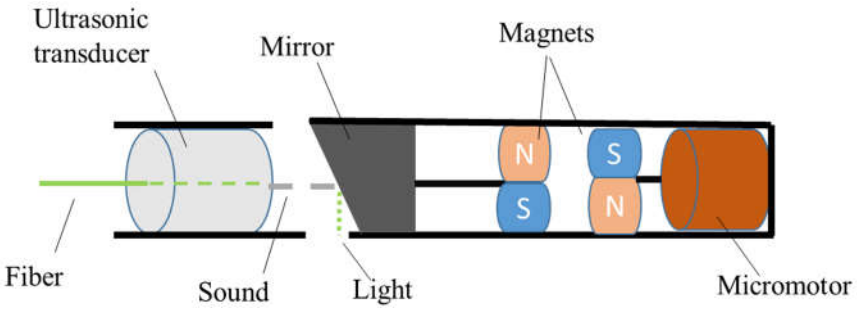

Fig. 1.5 Photoacoustic endoscopy (PAE)

The second biggest PA research field is PA gas [26] and aerosols [27-28] spectroscopy, which has mainly developed from 1995 to 2010. The published papers in this field are around half or one third of PAT. Approximately, 25% of published paper in photoacoustics come from this field. Main contents of this PA field is tracing and quantitative measurement of gas or aerosols concentration, for example urban air pollutants monitoring or safety alert in mine field. Some PA gas and aerosols spectroscopy equipment have already been commercialized. Another application is to detect gas emissions from grassland, fields or storage of fruits for agricultural applications. Common gas in agricultural applications include ammonia, ozone, alcohols and ethylene. Water vapor monitoring of food packaging is another topic. Infrared is common light source in this field [29], and PA cell design is one key of these implementations which is also important and may be used in other PA fields [30-31]. One of its new research trend is to adopt quantum cascade lasers for higher-performance gas tracing. Quartz were applied to optimize these system, called quartz-enhanced photoacoustic spectroscopy (QEPAS) [32-33]; Optical fiber were also adopted to enhance these designs.

Moreover, process analysis is another photoacoustic field [34-35], which has mainly been developed from 1975 to 2000. Comparing with the specific targets of PAT and gas or aerosols spectroscopy, this PA field includes many diverse interesting research topics, although the published papers are not large number. Only around 15% of published paper in photoacoustics come from this field. It is applied to analyze solid, semisolid and liquid non-destructively, including measurement of human tissue. Characterization of materials is a main topic, for example analyzing band gap, thermal diffusivity and thickness of different materials (semiconductors, polymer, paper, painting, thin films). It could be applied to characterize fossil fuels, monitor textile dyeing processes and contaminants in

water (for instance crude oil, hydrocarbons, thickness and depth profiles of biomass). Nanoparticles exhibiting strong optical absorption have been researched for PA contrast agent. Moreover, photoacoustic calorimetry for kinetic and thermodynamic measurements provide information of chemical transformations and inter- and intramolecular interactions [44]. Another topic is to apply photoacoustic method for noninvasive measurement of chromophore concentrations [36] in human tissue rather than imaging. Blood oxygenation, hemoglobin concentration [37] and glucose [38] are possible measurement targets. Also, noninvasive photoacoustic flow cytometry has been developed to detect cells or contrast agents in human tissue or plant vasculatures [39-40]. In addition, plants monitoring is another interesting topic, for example disease diagnosis of plants by analyzing gas emitting, leaf protein and absorbing-photon ability [41]. It could be applied for in vivo measurement of energy storage of plants by cyclic electron flow [42], and characterizing photochemical reactions, protein functions and dynamics in photobiology [43].

The above second and third PA field, gas, aerosols and process analysis could be classified as PA spectroscopy.

PA theory is another small PA fields [45], and has been mainly developed from 1985 to 2000. The published papers in this field take around 10% of all photoacoustic papers. In includes theory to characterize light-acoustics and light-heat transforming. Another topic is to analyze photoacoustic Doppler effect from flowing small particles with light absorbing or scattering ability [46-47].

Although the common terms are collected in difference applications, the PA systems are various according to application scenarios. For example, the equipment to measure gas chromophores are different with that for human tissue chromophores.

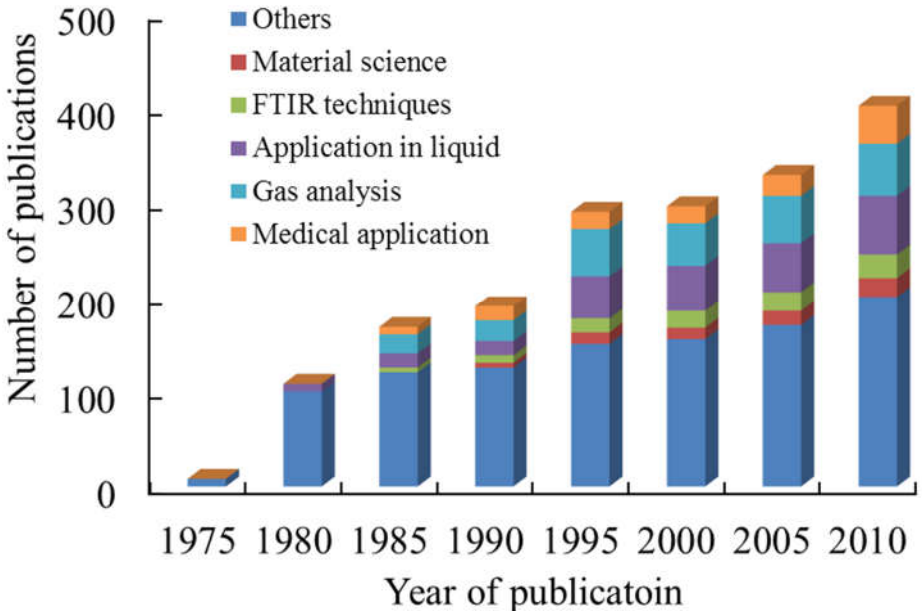

Fig. 1.6 Research development of PA spectroscopy

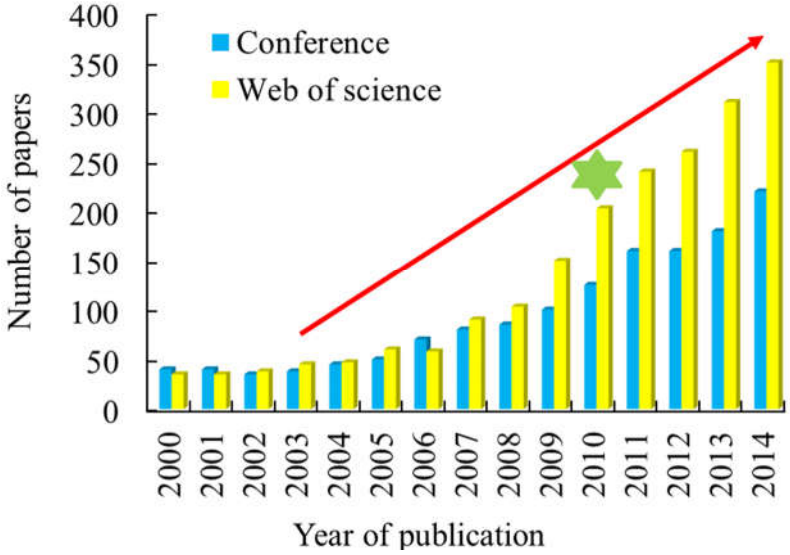

Fig. 1.7 Research development of PAT

Since 1975, the number of publications have been increasing obviously in all PA spectroscopy fields, as shown in Fig. 1.6 [48]. Since 2003, the published papers in photoacoustic tomography (PAT) have increased most dramatically. The published

papers every year have doubled roughly every three years. [49].Since 2010, PAT become the largest conference in 20,000-attendee Photonics West. Fig. 1.7 shows the development of PAT.

There are many research groups in the world already involved in photoacoustic research. USA, China and Japan are top 3 counties in photoacoustic research basing on the published paper. In USA, there are two leading groups for photoacoustic tomography. Prof. Lihong V. Wang's group in Washington University in St. Louis is one of them and they focus on brain activities, breast cancer and blood vessel observing. This group have corporation with companies Microphotonics and Endra Inc.. The University of Texas's group in USA focuses on breast cancer and supports SENO Medical Inc. to commercialize PAT equipment. Helmholtz Association in Germany mainly applies photoacoustic technique for skin cancer, and already corporates with company iThera Medical to launch its prototype of PAT. In Japan, there are Kyoto University and National Defense Medical College joining in this field. Their research targets focus on breast cancer and minimum blood vessel, and have corporation with Fujifilm and Canon Inc. respectively. Photoacoustics is an exciting and simultaneously practical filed. All these groups have cooperation with companies for commercial medical PA systems. Some PA imaging equipment have been commercialized recently [50]. Some other groups have developed imaging implementations for blood or blood capillaries by adopting appropriate wavelengths with strong absorbance from hemoglobin or other targets [51]. DNA and RNA are another possible targets. The optical wavelength of PAT changes according to measurement targets.

1.2.3 Motivation and objectives

Current major photoacoustic tomography (PAT) implementations are normally huge and expensive due to its pulsed laser, megahertz ultrasonic detection and mechanical system. These equipment are not suitable for many application cases. In gas and aerosols spectroscopy fields, PA systems have compact design. However, it cannot measure tissues, liquid and solid which are main demand in biomedical fields. The key of all PA research fields is to know optical absorption and PA signal sensitivity of measurement target. For example, recently exogenous contrast agent for PAT become hot topic. A cheap and portable equipment is needed for preliminary evaluation of contrast agent.

Table. 1.3 Novelty of this research comparing with photoacoustic tomography (PAT) implementations

Differences	Laser source	Detection	Aim
Current implementations for imaging system	Nanosecond pulse high-power laser system	High frequency ultrasonic wave (MHz)	Imaging
This research	Modulated continuous wave lower-power laser diode	Low frequency acoustic wave (kHz)	contrast agents evaluation

In this thesis, we proposed a compact photoacoustic system to meet this key measurement demand, which can confirm optical absorption and concentration of target non-destructively with high sensitivity. Table. 1.3 shows the novelty of this research comparing with major photoacoustic tomography (PAT) implementations. The system adopts dual laser diodes operated with modulated continuous waves and a MEMS

microphone at kilohertz region, which make the system cheap, small and compact. It may have a high level of application potential as portable evaluation equipment for materials, especially contrast agents in medical applications. Some kinds of ink solutions and contrast agents were used to confirm the possibility of the system.

1.3 Acoustic detector for photoacoustic system and related applications

1.3.1 Background and issues of acoustic detector

Photoacoustics mainly consist of optical excitation and acoustic detection. Here we provide a novel acoustic signal detection method and use it for sound intensity measurement.

Not only in photoacoustics but also other acoustic field, sound pressure distribution is a primary parameter. Normally, piezoelectric hydrophone is the conventional technique to detect acoustic signals [52-53]. There are some other available tools, for example fiber optic hydrophone [54-59] and Schlieren method [60-62]. In acoustics, we can also use sound intensity to characterize acoustic field. Sound intensity is a vector quantity which can provide both direction and magnitude of sound energy flow [63], while sound pressure is scalar and can only provide the information of magnitude. Sound intensity could provide some advantages in application, for example: qualifying the sound power generated by any one of several acoustic sources simultaneously; confirming travelling wave or standing wave dominate; finding key sound source; understanding how absorber or reflectors work. Thus it can greatly enhance the efficiency and precision of acoustic

control.The usual application for sound intensity measurement now is to monitor noise sources in air, which is already commercialized. Sound intensity measurement underwater were also developed using piezoelectric hydrophone rather than condenser microphone [64-66].

Normally, sound intensity detection needs several sensors because it requires both particle velocity and sound pressure information. Two sound pressure sensors are needed to confirm practical velocity which is deduced from the gradient of pressure. When testing intensity vector in two or three dimensions, we need four or six press sensors. As a result, the increasing number of coaxial cables are required in practical sound intensity test. Both number and length of metal cables limit the practical intensity measurement in water, which makes intensity measurement impossible in the case of huge water tank in factories used in industrial applications. Because the electronic components of the instrument should be placed in the dry area and require a longer transmission distance. With the increasing of sensors, the practical measurement systems becomes larger, heavier and has shorter transmitting distance due to the high output electrical impedance matching problem of coaxial cables.

1.3.2 Motivation and objectives

Here we provides a novel design for acoustic detector and sound intensity probe under liquid in ultrasonic field. This sensor consisted of light emitting diode (LED), piezoelectric (PZT) element and plastic optical fiber (POF) [67-69]. PZT element converts sound pressures to electric voltage, which change the optical signal of LED correspondingly. Then optical signals are transmitted by POF and analyzed by photo detectors. Finally, we could know the acoustic signals by optical signals. We call this

new-design as LED-PZT sensor. This technology shall make acoustic measurement smarter since extending of cable length and weight of the sensors have little limitation.

In order to confirm the operation of the proposed LED-PZT sensor, the experiments were demonstrated to measure sound pressure by single sensor and sound intensity by four sensors in ultrasonic field under water. This novel configuration of acoustic detector has wide applications in industry for high-intensity ultrasound under liquid, for example ultrasonic imaging, heightening chemical reaction and cleaning.

Moreover, this research may be used for photoacoustic measurement. Basically human body is water in physics. In order to increase the impedance match, photoacoustic spectroscopy and imaging in medical application mainly are implemented under water. Adopting this LED-PZT sensor, the whole photoacoustic system could be connected by fiber. The measurement system become smaller, lighter and longer transmitting distance.

1.4 The organization of thesis

This thesis aims to develop photoacoustic system for contrast agent evaluation in biomedicine applications, and to develop acoustic detector array for photoacoustic system and related acoustic application.

In order to achieve these objectives, this thesis is divided into five chapters, includes this introduction. The thesis organization is illustrated in Fig. 1.8.

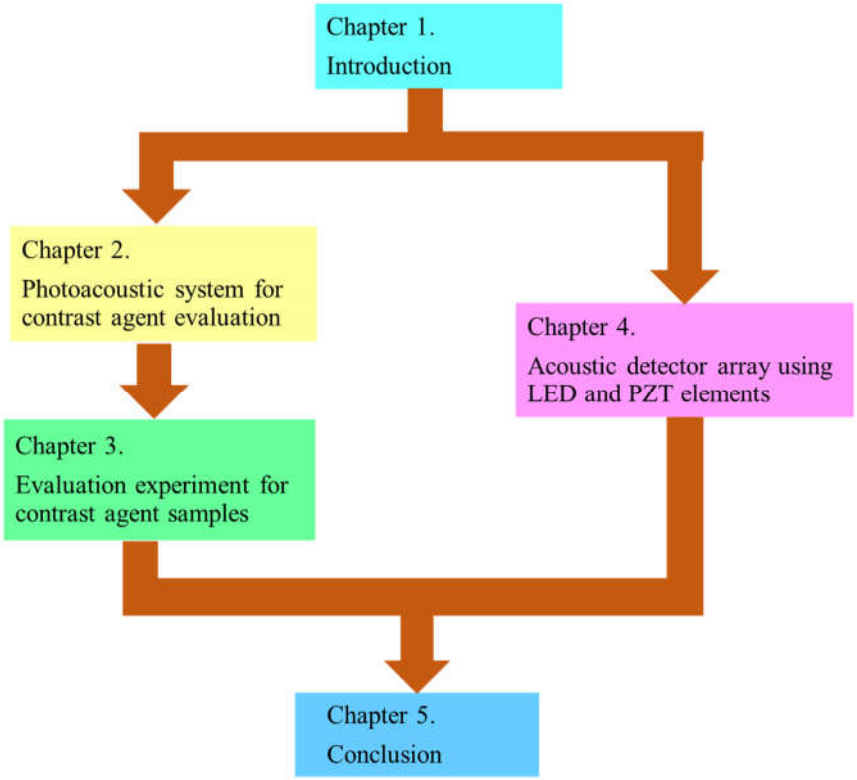

Fig. 1.8. The organization of thesis

In chapter 2, we propose a portable photoacoustic (PA) system, which can work as a common non-destructive evaluation equipment for PA material. The theoretical and practical characteristics of PA system are described. Some ink solutions and wood were tested to confirm the possibility of the system.

In chapter 3, we apply this PA system for contrast agent evaluation in biomedicine. Some contrast agents, including ICG and TO-001 solution, are measured to confirm the high sensitivity of PA system. Further characteristics of this system are tested by contrast agent evaluation too.

In chapter 4, we develop a novel acoustic detector array for PA system and related acoustic application. The detector consists of LED and PZT, and transmit signal by fiber. The detector array is used to measure sound pressure and sound intensity distribution in

an ultrasound field, and presents its effectiveness and advantages comparing with conventional acoustic detector array.

Finally, in Chapter 5, we introduce the main conclusions of this thesis and explain the remaining problems and ideas for the future work.

Chapter 2

Compact photoacoustic system for sensitivity evaluation of materials

Modern photoacoustics has been developed in the past 40 years and applied in different fields. However, most of implementations are large and expensive. In this chapter, a compact and cost effective PA system has been developed for sensitivity evaluation of materials, especially for PA contrast agent.

2.1 Fundamental of PA system

Modern PA theory for solid and semisolid matter was described by Rosencwaig and Gersho in 1976, called Rosencwaig–Gersho theory [70]. This theoretical model distinguishes PA phenomena to six different cases according to the relationship between sample length, thermal diffusion length and optical absorption length [71].

Optical absorption length u_β has reciprocal relationship with sample absorption β (cm^{-1}) as below:

$$u_\beta = \frac{1}{\beta}. \tag{2.1}$$

Thermal diffusion length of sample u_s is determined by equation below:

$$u_s = \frac{1}{a} = \sqrt{\frac{2 \cdot \alpha_s}{f}} . \tag{2.2}$$

a is the thermal diffusion coefficient of sample (cm^{-1}), and f is modulation frequency.

a_s is thermal diffusivity of sample (cm^2/sec) and is determine by equation below:

$$\alpha_s = \frac{k_s}{\rho_s C_s} \tag{2.3}$$

k_s, thermal conductivity of sample ($cal/cm \cdot \sec \cdot ℃$); ρ_s, density of sample (g/cm3);

C_s, the specific heat of sample ($cal/g \cdot ℃$). The thermal diffusivity of water is 0.00143 cm^2/s. According to equation (2.2), we can calculate the thermal diffusion length of water are 0.00085 and 0.00061 cm when the modulation frequency are 4 and 7.8 kHz respectively.

In this chapter, thermal diffusion length of the sample solution is basically equal to water (≈ 0.0006 cm) due to its the low concentration (＜0.2%). So the thermal diffusion length of sample is much shorter than the depth of the sample solutions (≥ 4 cm). Laser beam penetrate through the whole sample, as shown in Fig. 2.1.

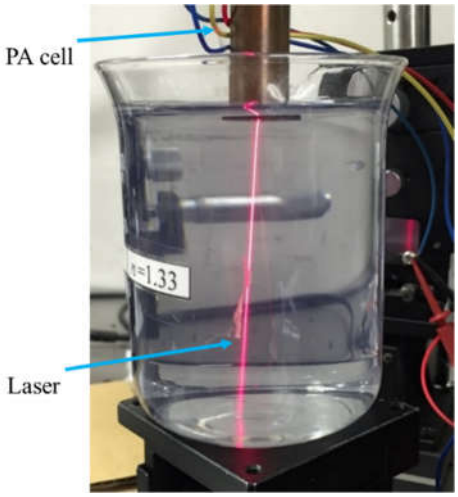

Fig. 2.1 Laser beam penetrate through the sample solution.

Thus, in this chapter, the relationships among three key parameters of sample solutions are shown as below for coming experiments,

$$u_\beta > l > u_s , \tag{2.4}$$

where u_β is the absorption length in sample (cm), l is the depth of sample (cm), , and u_s is the thermal diffusion length of sample (cm).

Moreover, PA signal is determined by the equation below [70]:

$$PAS = -j\frac{\beta \cdot u_S \cdot u_S}{2 \cdot \alpha_g \cdot k_s} \cdot \frac{\gamma \cdot p_0 \cdot I_0}{2\sqrt{2} \cdot l_g \cdot T_0}, \tag{2.5}$$

j is the imaginary unit. In practice, we only consider the imaginary part and don't need to consider the imaginary unit. r is the ratio of the specific heats in adiabatic law of gas

$$PV^r = const , \tag{2.6}$$

P is the pressure, while V is the gas volume in the cell. β, the optical absorption of sample (cm^{-1}); u_s, thermal diffusion length of sample; α_g, the thermal diffusivity of

gas (cm^2/sec); k_s, thermal conductivity of sample ($cal/cm\cdot sec\cdot ℃$); p_0, the ambient pressure; I_0, the incident monochromatic light flux (W/cm^2); l_g, length of gas; T_0, the actual temperature of sample surface (℃), which consists of ambient temperature plus the increasing temperature from the absorbed heat of input light.

Normally, the PA signal equation is simplified as below:

$$PAS \propto \frac{I_0 \cdot \beta \cdot u_S}{f^{\frac{3}{2}}}. \tag{2.7}$$

Here, f is the modulation frequency (kHz) [71]. Moreover, according to Beer–Lambert law [72], we have relationship as below:

$$\beta(\lambda) \propto \varepsilon(\lambda) \cdot c \tag{2.8}$$

$\varepsilon(\lambda)$ is absorption coefficient ($L \cdot mol^{-1} \cdot cm^{-1}$) and c is concentration of sample (mol/L). By equation (2.7) and (2.8), photoacoustic Beer–Lambert law could be deduced as below:

$$PAS \propto \frac{I_0 \cdot \varepsilon(\lambda) \cdot c \cdot u_S}{f^{\frac{3}{2}}}. \tag{2.9}$$

In one case, the sample is tested by two different optical wavelengths λ_1 and λ_2. Other parameters are set as the same in the experiment, for example optical power of two wavelengths and modulation frequency etc. The PA signals of two wavelengths should have relationship as below:

$$\frac{PAS(\lambda_1)}{PAS(\lambda_2)} = \frac{\varepsilon(\lambda_1)}{\varepsilon(\lambda_2)}. \tag{2.10}$$

In another case, the concentration of sample change from c_1 to c_2, and other parameters are set as the same. According to equation (2.9), the PA signal is only

determined by the concentration of sample.

$$\frac{PAS_1}{PAS_2} = \frac{c_1}{c_2}. \tag{2.11}$$

In this way, the concentration of sample can be confirmed.

Moreover, if we use two different optical wavelengths λ_1 and λ_2 to measure mixture of two materials, we could get two equations as below.

$$PAS(\lambda_1) \propto \varepsilon_1(\lambda_1) \cdot c_1 + \varepsilon_2(\lambda_1) \cdot c_2 \tag{2.12}$$

$$PAS(\lambda_2) \propto \varepsilon_1(\lambda_2) \cdot c_1 + \varepsilon_2(\lambda_2) \cdot c_2 \tag{2.13}$$

Then the mixture ratio of two materials could be deduced.

2.2 Design of PA system

We have designed compact PA system, as pictured in Fig. 2.2. We employ two laser diodes (LD) with 660 nm and 785 nm wavelength as excitation sources (660 nm LD, MITSUBISHI ML101J27; 785 nm LD, THORLABS L785P090). The samples are irradiated with average optical power of approximately 20 mW and the spot size of the LDs is collimated to 5.0 mm by lens. The LDs are modulated by a function generator (Tektronix, AFG310) via a proper resistor providing 100% depth rectangular modulated voltage. The LDs could be changed by a switch. A polarization beam splitter (PBS, dimension: 20 X 20 X 20 mm) combines the two collimated laser beam. Beams pass through the PA cell, which works as a resonator to amplify photoacoustic signal. Then beams are absorbed by sample. It leads to the generation of acoustic signal in the coupling gas (air), which was detected using a Micro Electro Mechanical Systems (MEMS) microphone (1.45(H) X 6.15(L) X 3.76(W) mm, Knowles-acoustics, SP0103NC3-3). PA

cell is made by copper and microphone locate in the middle of cell. The uniform frequency of microphone is from 100 Hz to 10 kHz. Finally, a preamplifer (NF corp., 3611) and a lock-in amplifier (NF corp., 5560) are adopted to process the PA signal. Fig. 2.3 shows the pictures of PA system.

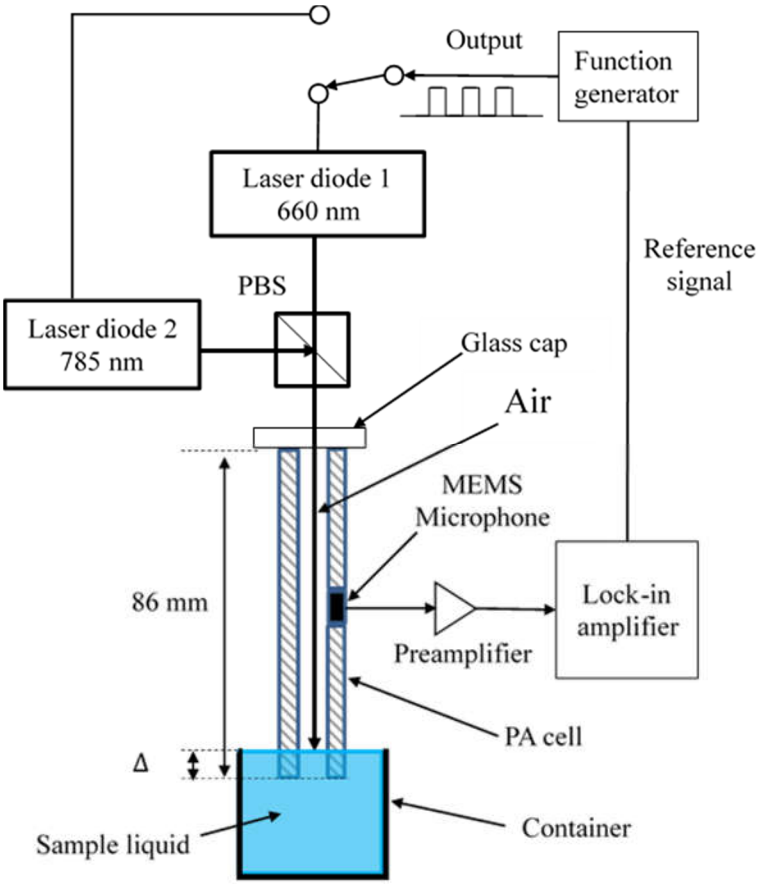

Fig. 2.2 The proposed compact PA system.

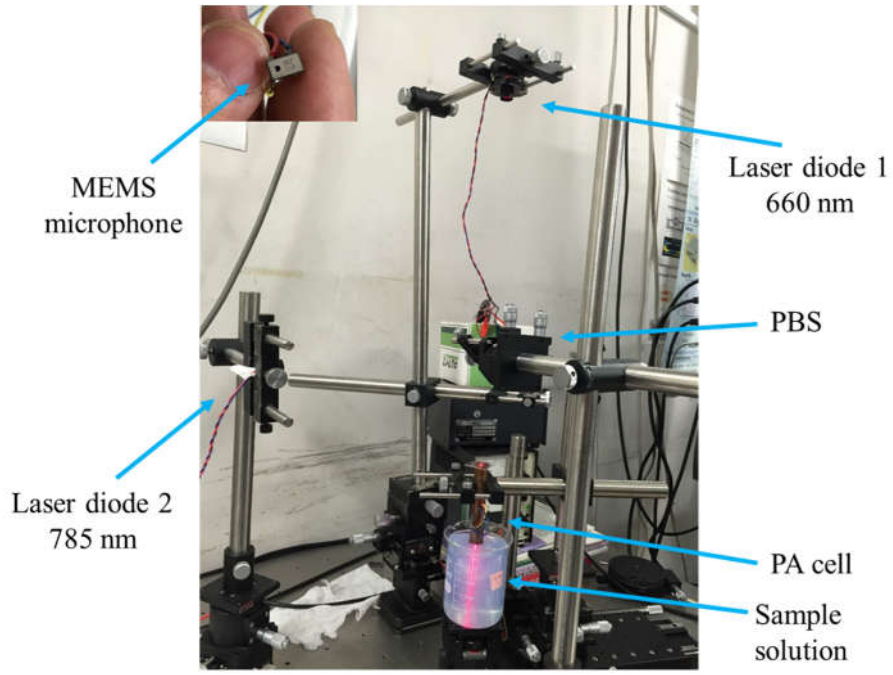

Fig. 2.3 Picture of PA system.

2.3 Design of PA cell

2.3.1 Theoretical design and processing factors

The PA cell in Fig. 2.2 has a cylindrical shape with the inner volume of 1688 mm^3 (external diameter = 15 mm; internal diameter = 5 mm and height = 86 mm), and made of copper. The inner surface is polished to minimize spurious PA signal considering the absorption on the wall. The top of the PA cell is sealed with a glass plate and the bottom is dipped at the sample surface. Therefore the cell could amplify PA signal by working as a fixed-fixed acoustic resonator. The microphone is fixed at the center of PA cell to use the pressure loop of resonance modes.

The working frequency of microphone is 0.1-10 kHz, which means the minimum acoustic wavelength is 34 mm considering acoustic speed as 340 m/s. According to the

acoustics theory, this cylindrical resonator meets equation below

$$\frac{d}{\lambda} < 0.5, \tag{2.14}$$

d is the diameter of PA cell and λ is wavelength of acoustic signal. Therefore, PA cell could be treated as one-dimension resonant tube. Moreover, one-dimension fixed-fixed acoustic resonator meets equation below [73]:

$$\lambda_n = \frac{2L}{n} \qquad (n = 2,4,6.....). \tag{2.15}$$

L is length of PA cell. We also have the relationship $f = c/\lambda$. f is acoustic frequency. c is the acoustic speed in air (340 m/s). Then the relationship between acoustic frequency f and length of PA cell L could be deduced as below:

$$f = \frac{nc}{2L} \qquad (n = 2,\ 4,\ 6\ldots\ldots) \tag{2.16}$$

According to equation (2.16) and equation for acoustic speed c

$$c = 331 + 0.6 \cdot T, \tag{2.17}$$

characteristics of PA cell could be calculated as table 2.1. Here T is the centigrade temperature of ambient temperature.

From table 2.1, when n is 2 and environment temperature increasing from 20 to 25 ℃, the best modulation frequency increases by 0.035 kHz theoretically. At the same case, the best modulation frequency increases by 0.07 kHz when n is 4. In the case of n equal to 2, when environment temperature changing by 10 ℃ and the length of PA cell changing by 2 mm, the best modulation frequency changes by 0.15 kHz. At the same case, the change of best modulation frequency should be double when n is 4 comparing with n equal to 2.

Table 2.1 Characteristics of PA cell

n	Length of PA cell	Length of PA cell	Acoustic wavelength	Environment temperature	Acoustic speed	Frequency
	mm	m	(m)	(℃)	(m/s)	kHz
2	86	0.086	0.086	20	343	3.9884
2	86	0.086	0.086	25	346	4.0233
2	86	0.086	0.086	30	349	4.0581
2	85	0.085	0.085	20	343	4.0353
2	85	0.085	0.085	25	346	4.0706
2	85	0.085	0.085	30	349	4.1059
2	84	0.084	0.084	20	343	4.0833
2	84	0.084	0.084	25	346	4.1190
2	84	0.084	0.084	30	349	4.1548
4	86	0.086	0.043	20	343	7.9767
4	86	0.086	0.043	25	346	8.0465
4	86	0.086	0.043	30	349	8.1163
4	85	0.085	0.0425	20	343	8.0706
4	85	0.085	0.0425	25	346	8.1412
4	85	0.085	0.0425	30	349	8.2118
4	84	0.084	0.042	20	343	8.1667
4	84	0.084	0.042	25	346	8.2381
4	84	0.084	0.042	30	349	8.3095

There are several factors should be considered when designing PA cell. The first factor is the loss processes inside the PA cell to reduce acoustic signal. One main loss is the standing wave interacts with the internal surface of PA cell, for example viscous and thermal loss near to internal surface.

Spurious PA signal is another factor should be considered for PA cell design. Spurious PA signal does not result from optical absorption of sample, but from other parts, for example PA cell or entrance window. It cannot provide the sample information and be removed from real PA signal, which become serious problem when this spurious PA

signal is high. There are several conditions have relationship with spurious signal. Absorption coefficient of PA cell material and entrance window should be low in order to reduce spurious signal. Moreover, diameter of PA cell should be larger or similar to diameter of laser beam. Inner surface of PA cell had to be polished for less optical scattering from wall and microphone, which shall increase spurious signal too. We should use non-absorbing gas in PA cell, and clean the windows and inner surface of cell before measurement.

The mechanical property of PA cell material is another factor to consider too. The mechanical property of PA cell material should be difference with that of its inside. For example, density and Young's modulus of PA cell should be much higher than its inside to increase acoustic impedance for better resonance. Here the material of PA cell, copper, has big difference comparing with its inside air. Moreover, copper is stable and not easy to be oxidized.

2.3.2 Test of PA cell

2.3.2.1 Resonant frequencies of PA cell tested by ink solution

We used experiment setup (Fig. 2.2) to measure resonant frequencies of PA cell. 785 nm laser diode worked as laser source. Black ink solution (45 mg/dl) worked as sample. Firstly, we changed the modulation frequency of function generator by a step of 0.1 kHz from 0.1 to 12.0 kHz to find the rough resonant frequencies. Resonant frequencies of this PA cell are approximately 4, 8 and 12 kHz respectively, which meet the equation (4), as shown in Fig. 2.4 (a). In order to get higher and more stable amplification, 8 kHz was chosen as working frequency, considering the working frequency of microphone is from

0.1 to 10 kHz in specifications. Signals observed at very low frequencies should be spurious signal because of the electronic system. Secondly, we reduced the step of modulation frequency to 0.02 kHz for precise resonant frequency around 8 kHz. We may observe resonance with finer frequency step 0.001 or even 0.0005 kHz by actual demand. Fig. 2.4 (b) show the result. Finally, we found the peak at 7.78 kHz, which is the two-wavelength resonant frequency of the PA cell. Q of the resonance is approximately 40.

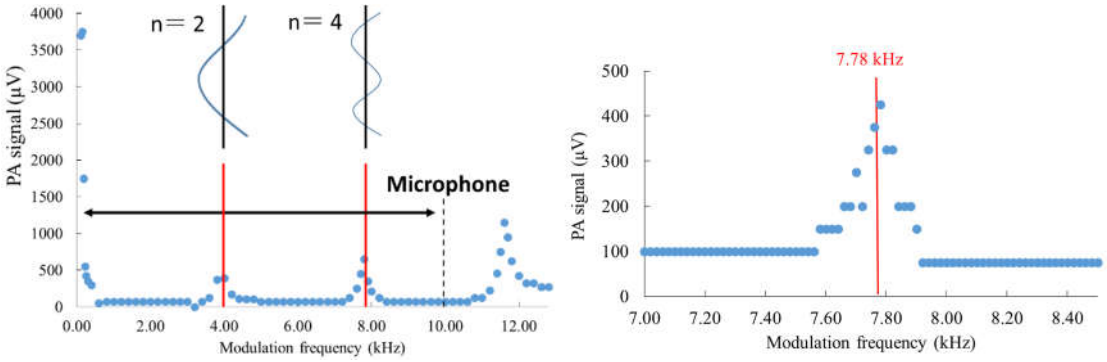

(a) **(b)**

Fig. 2.4 Resonant frequencies of PA cell tested by black ink solution and 785nm LD.

In actual measurement, peak PA signal locating at around 4 or 8 kHz is not sure in the working frequency of microphone from 100 Hz to 10 kHz. Sometimes the peak located at around 4 kHz, while the others around 8 kHz. Fig. 2.5 shows another test of resonant frequencies of PA cell by black ink solution and 785nm LD. The maximum PA signal located at around 4 kHz, which was different with Fig. 2.4. According to equation (2.7), PA signal will decrease while modulation frequency increasing. It means PA signal at around 4 kHz should higher than that at around 8 kHz. However, the actual situations are more complicated. Characteristics of PA cell should be considered too. Although the dimension of PA cell meets equation (2.14) and could be treated as one-dimension

resonant tube, it is not ideally one-dimensional. Acoustic signals oscillate from one end to another end of PA cell along vertical axis to form resonance. At the same time, acoustic signal transmit along horizontal axis. Normally, higher frequency results in higher transmitting loss. In the case of high frequency, acoustic signals change dramatically near to the middle of PA cell. PA signals is more sensitive with position change. This is the reason why the peak PA signal sometimes locates at around 4 kHz and sometimes locates at around 8 kHz.

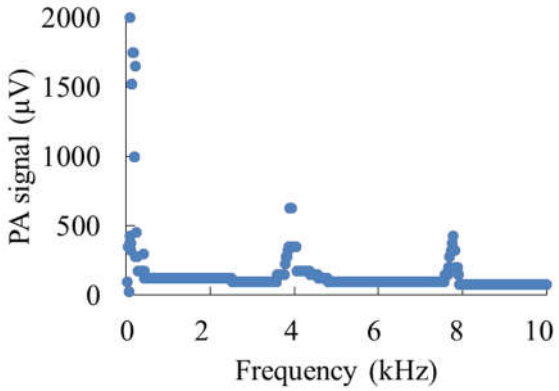

Fig. 2.5 Another test of resonant frequencies of PA cell by black ink solution and 785nm LD.

2.3.2.2 Reflection coefficient of sample vs. resonant frequency of PA cell

Here we will confirm if resonant frequency of PA cell change by the reflection coefficient of sample. Reflection coefficient R between two materials was determined by equation as below:

$$R = \frac{Z_1 - Z_1}{Z_1 + Z_1}. \tag{2.18}$$

Z_1 is the acoustic impedance of gas inside PA cell. Here is air. Z_2 is acoustic impedance of tested sample. Acoustic impedance Z of some material is determined by equation below:

$$Z = \rho \cdot c \tag{2.19}$$

ρ is density of material and $c$is the sound speed of this material. According to two equations above, we can calculate the reflection coefficients between air and water, between air and wood, and between air and glass are 99.95%, 99.96% and 99.99% respectively. Table 2.2 shows the details. The reflection coefficient changes little although the samples are changed from water to wood and glass. So the resonant frequency change little although we change the sample from water to wood and glass. However, we should know that the resonant frequency is determined by many factors in practical case, for example the air length inside PA cell, temperature and humidity etc. Here we only consider the case when only changing the density of sample.

Table 2.2 Reflection coefficient of sample

	Air	Water	Wood	Glass
Density (kg/m3)	1.1839	997.0479	500	2500
Speed of sound (m/s)	346.13	1,507	3960	3962
Acoustic impedance (Pa·s/m)	409.4	1502551.2	1980000	9905000
Reflection coefficient	air-water 99.95%	air-wood 99.96%	air-glass 99.99%	

2.4 Test of PA system characteristics

2.4.1 Absorption spectrum of ink samples

In order to verify the proposed PA system, we measured ink solutions. Fig. 2.6 shows absorption spectrum of ink samples detected by a spectrometer, including black ink (PILOT, Black ink, 30 ml), dye ink (Hobby&Creation, 水性エナメル, 25 ml) and water.

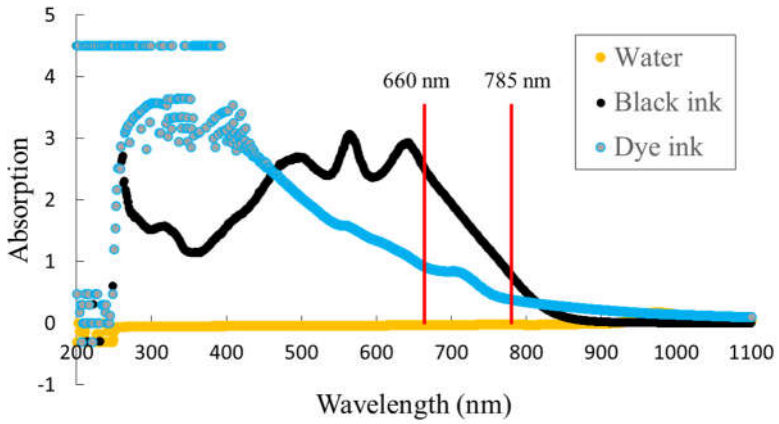

Fig. 2.6 Absorption spectrum of samples measured by spectrophotometry.

Table 2.3 Optical absorption for water and inks.

Wavelength (nm)	Optical absorption coefficient (cm-1)		
	Water	Black ink	Dye ink
660	0.004	754.71	228.45
785	0.01	203.41	90.47
Ratio (660/785)	0.4	3.7	2.5

These materials will work as samples in the experiments. In order to distinguish mixture percentage of the black ink to the blue ink, we adopted LDs with 660 and 785 nm. Ratios between absorption coefficient at 660 nm and that at 785 nm are about 3 for either ink.

Absorption of water is almost zero no matter at which wavelengths. Table 2.3 shows the summary of these absorption and ratios.

2.4.2 Modulation duty vs. PA signal

We investigate how PA signal change by the change of duty ratio of the modulation for the LDs. Water and black ink solution (45 mg/dl) were used as sample. The 785-nm LD worked as laser source. Fig. 2.7 shows the measurement results.

The output PA signal increased linearly with duty ratio, and reached the maximum when the duty ratio is 50%. Here we confirm that the setup is working with the continuous excitation, and the output signal reach the maximum when the cooling period is same as the heating period.

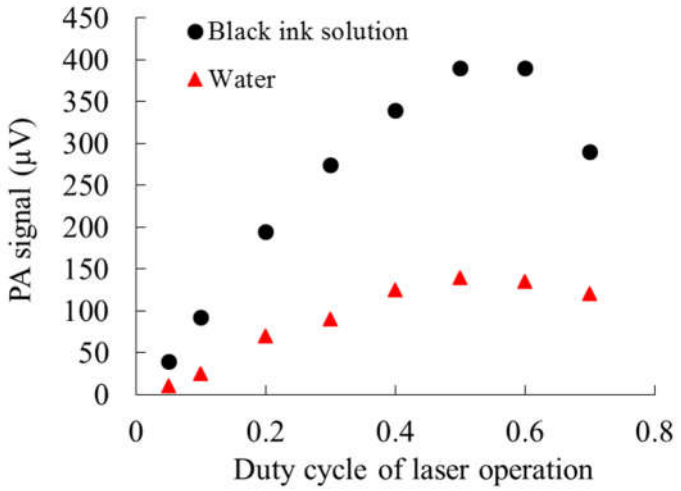

Fig. 2.7 Duty ratio of the light source and PA output level.

2.4.3 Depth of sample into the PA cell vs. PA signal

As shown in Fig. 2.8, the depth of sample was increased gradually into PA cell and we test how the PA signal changed. The air length in PA cell reduced by length Δ

correspondingly. According to equation (2.15), the middle of air length in PA cell has the maximum sound pressure. Moreover, microphone is fixed at the middle of PA cell. While Δ increasing, the microphone gradually stay away from the location of maximum sound pressure. Therefore the output PA signal shall decrease correspondingly.

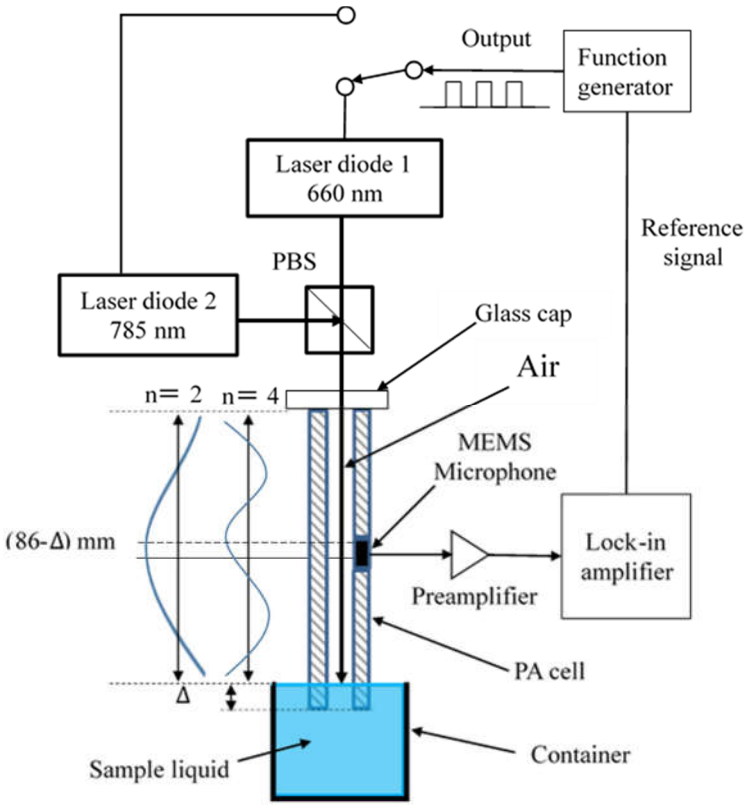

Fig. 2.8 Depth of sample into PA cell .

Fig. 2.9 shows the measurement result. The PA signal reduced almost linearly with the increase of the length Δ. All these peaks were achieved when resonant frequency is 3930 kHz.

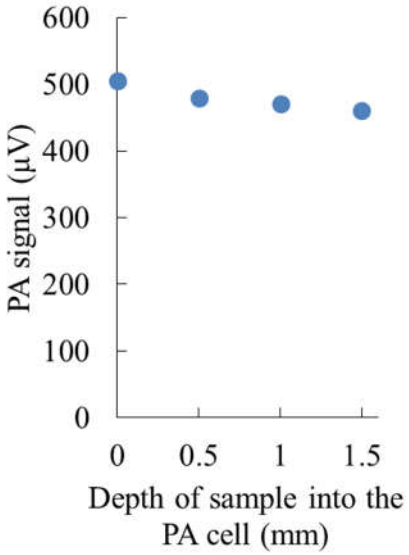

Fig. 2.9 Depth of sample into PA cell vs. PA output level by measurement.

According to the distance between peak PA signal and center of microphone in Fig. 2.8, we can deduce equations for PA signal:

$$PA\ signal = A\cos\left(\frac{\Delta/2}{86-\Delta}\cdot 2\pi\right) \quad (n=2) \tag{2.20}$$

$$PA\ signal = A\cos\left(\frac{\Delta/2}{\frac{(86-\Delta)}{2}}\cdot 2\pi\right) \quad (n=4) \tag{2.21}$$

A is the maximum PA signal when the length Δ is 0 and air length inside PA cell is 86 mm. By equation (2.20) and (2.21), the theoretical PA signals change by depth of sample into PA cell could be calculated and plotted as Fig. 2.10. When n=4, PA signal reduced more comparing with n=2. The actual measured PA signal in Fig. 2.9 reduced more dramatically, while the theoretical calculation results have little changed as Fig. 2.10. Because actual errors are not included in theoretical calculation, for example the actual position of microphone, precise control of depth of sample into PA cell etc.

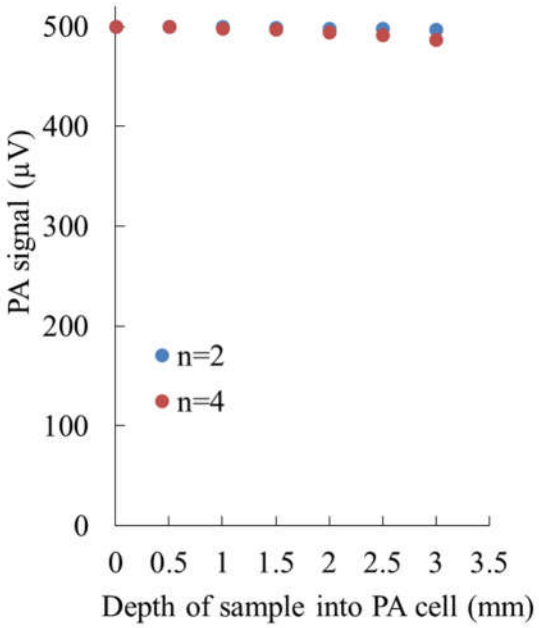

Fig. 2.10 Depth of sample into PA cell vs. PA output level by theoretical calculation.

2.5 Evaluation of concentration and mixture ratio of ink solution samples

2.5.1 PA signal vs. concentration of black ink

Black ink were gradually added into the water sample (height, 7.8 cm; volume, 2.35 dl) with a step of 10 mg/dl to increase the concentration of the ink solution. Fig. 2.11 shows how this PA system confirm the concentration and absorption of black ink solution. The average optical power for 660 and 785 nm are both 20 mW. When the sample was water (0 mg/dl), the PA signal for 785 nm was higher than that for 660 nm. Because the absorption coefficient of water at 785 nm is higher than that at 660 nm. Here we know this PA system is quite sensitive and can tell small difference of absorption, which is key requirement for PA system. However, the PA signal ratio at two wavelengths is not same as absorption

coefficient ratio of water. Because these low signals were affect by the system noise. As for the ink solutions with concentration from 10 to 50 mg/dl, the PA signal at both wavelengths increased linearly with concentration increasing, and the signals of 660 nm was always around three times of that of 785 nm. All other parameters affecting PA signal were kept the same, for example optical power, environment temperature. So PA signal here is decided only by the optical absorption coefficient. The measurement results above agreed well with equation (2.11), photoacoustic Beer–Lambert law, and also agree well with the absorption coefficient ratio between 660 and 785 nm shown in Table 2.3.

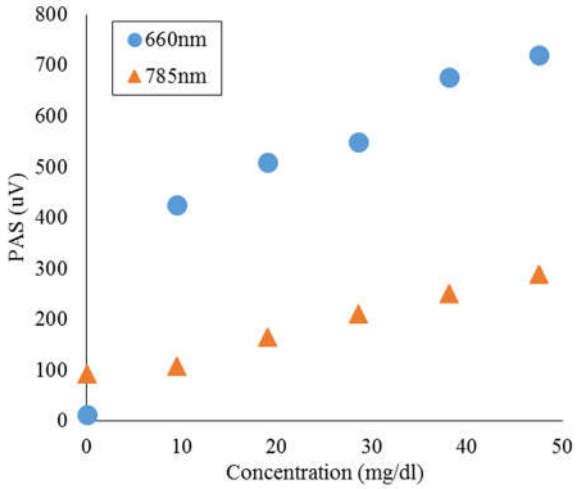

Fig. 2.11 PA signals at 660 and 785 nm vs. concentration of black ink solution.

2.5.2 PA signal vs. mixture of black ink and dye ink

In second experiment, six groups of samples were prepared as shown in Table 2.4. The sample group 0 is water and other samples are ink solutions mixed with black ink and dye ink. The results are shown in Fig. 2.12. The PA signals of Group 0 were same as last experiment. From group 1 to 5, weight of black inks were reduced, while that of dye ink were increased. PA signal at both wavelengths reduced correspondingly, since absorption

coefficient of black ink is higher than that of dye ink at both 660 and 785 nm. To identify the mixture ratio of two inks is another key results. We calculated and plotted the signal ratio between that at 660 nm to 785 nm in the figure. Ratio of group 0 is smaller than 1, while ratio of other group are larger than 1. From group 1 to 5, signal ratio reduced gradually by mixture ratio because absorption ratio of black ink between two wavelengths is larger than that of dye ink. The weight mixture ratio of the black ink to the dye ink can be found by the signal ratio successfully, which meet photoacoustic Beer–Lambert law as equation (2.12) and (2.13) too.

Table 2.4 Samples with black and dye ink mixed into water of 0.5 dl.

Sample group	0	1	2	3	4	5
Black ink (mg)	0	200	150	100	50	0
Dye ink (mg)	0	0	50	100	150	200

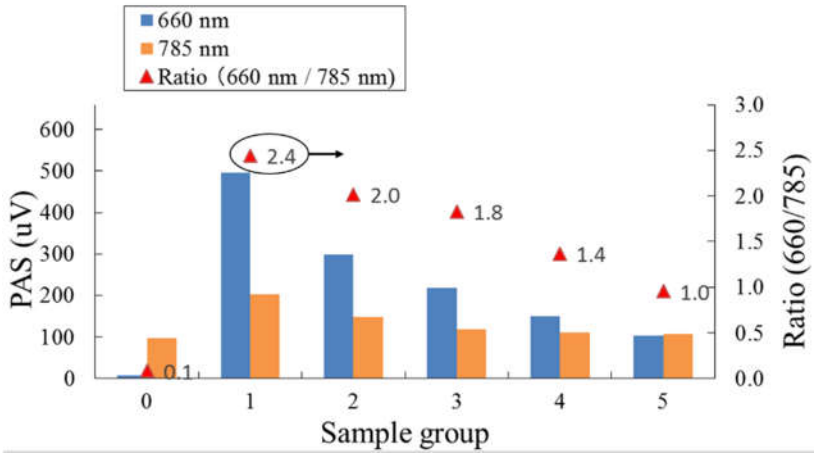

Fig.2.12 PA signals for mixtures of black and dye ink at 660 nm and 785 nm.

2.6 Evaluation of wood

After measuring the liquid sample, the solid sample was tested in this part. A piece of wood with 10 mm thickness worked as sample here. Fig. 2.13 shows the picture of experiment. The wood was pressed up against one end of PA cell that no light could be seen between the wood and PA cell. It means that one end of PA cell is sealed well by this wood.

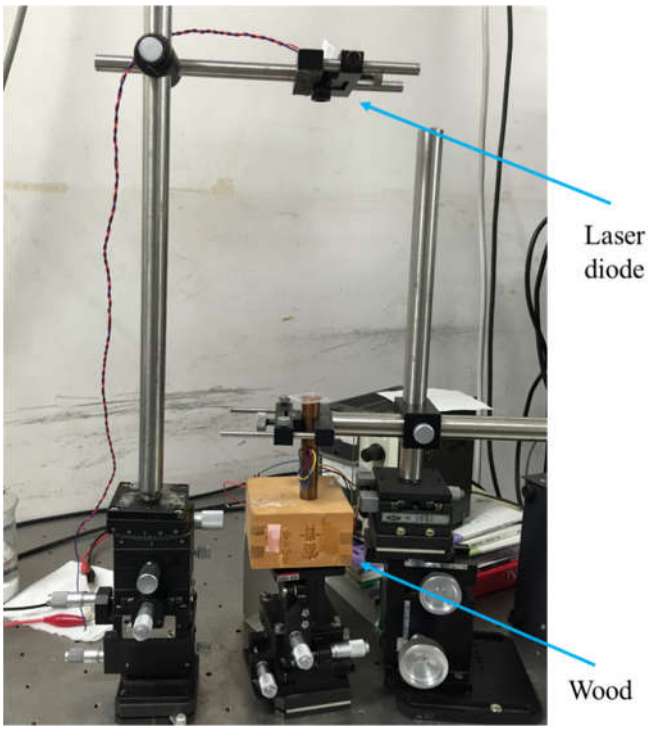

Fig. 2.13 Picture of wood testing.

As mentioned above, the relationships between sample length, optical absorption length and thermal diffusion length of sample are the key of photoacoustic measurement. Unfortunately, we don't know the actual optical absorption length and thermal diffusion length of sample of this wood. So we can't confirm the relationship between these three

parameters and the measurement equation. However, if the absorption of wood is high enough to form PA signal, the peak PA signal should be found when it reaches resonant frequency of PA cell. PA signal should be linear with optical power of light source when diameter of laser focus is fixed, no matter which case. The two experiments below were implemented to confirm these two basic characteristics of wood.

As shown in Fig. 2.14, the peak PA signals were found when modulation frequencies were around 4, 8 and 12 kHz at both 660 and 785 nm, which meet the one, two and three wavelength resonant frequency of the PA cell. When modulation frequency was 11.8 kHz, both PA signals of 660nm and 785nm reached maximum. The peak PA signals at 785 nm were around two times of that at 660 nm. The thermal diffusivity of water at 25 ℃ and wood of yellow pine are 0.00143 and 0.00082 cm^2/s respectively. By this, we could calculate the thermal diffusion length of these two materials are 0.0006 and 0.0005 cm respectively. The thermal diffusion length of water is little longer than that of yellow pine. We assume all woods have similar thermal diffusion length. The peak PA signals of wood were around 4 and 10 mW, while that of ink solutions were less than 1 mW. PS signal of wood is several times of that of ink solutions. We could deduce the optical absorption of this wood should be much larger than that of ink solution we measured before. Because other factors of two measurements were similar and the PA signals should be determined by optical absorption. The average optical powers of 660 and 785 nm laser were 19 and 34 mW respectively and the diameters of both laser focus were around 5 mm.

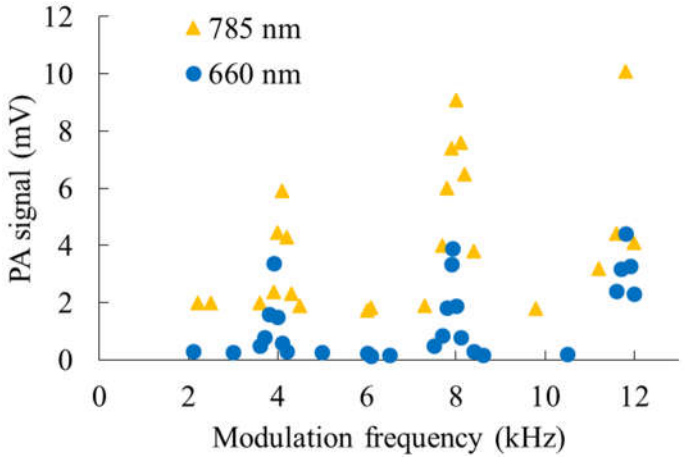

Fig. 2.14 PA signals vs. modulation frequency at 660 and 785 nm.

Then we measure the PA signal when changing optical power of lasers. As shown in Fig. 2.15, PA signals increased linearly with average optical power of 660 nm and 785 nm. The slope of 785 nm line is much larger than that of 660 nm. It means PA signal at 785 nm increase more obviously with optical power than that at 660 nm. Here the average optical power of 785 nm laser is around two time of that of 660 nm laser. The diameters of both wavelengths are always around 5 mm. The resonant frequency of both wavelengths is 7.89 kHz. According to the trend of lines, the PA signal of 785 nm should be higher than that of 660 nm when the average optical power is the same. By this experiment result, we can deduce that the absorption coefficients of wood at 785nm is higher than that at 660nm. Because all other factors were the same, for example temperature, humidity, thermal diffusion length etc. PA signal is determined by optical absorption coefficient.

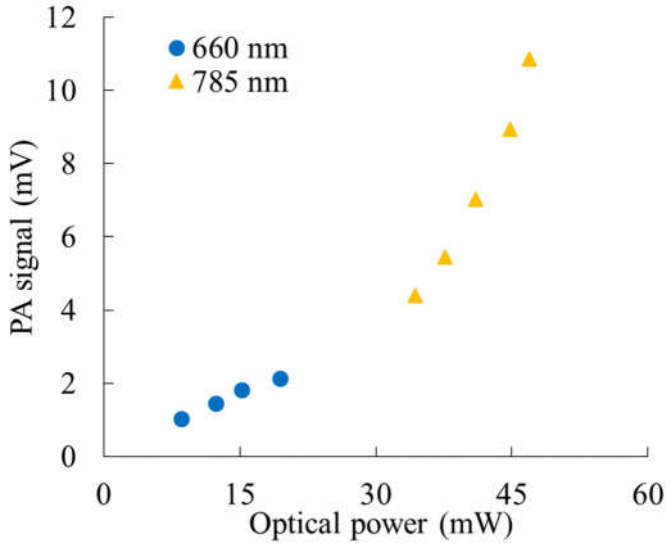

Fig. 2.15 PA signals vs. optical power at 660 and 785 nm.

2.7 Conclusions

We designed a portable and cost effective photoacoustic system adopting continuous optical excitation at low modulation frequency for providing a universal PA system for material evaluation, including liquid and solid. Different ink solutions and a piece of wood were tested to confirm its performance and high sensitivity. According to the main results, this PA system with two laser wavelengths can test concentration and mixture ratio of single or two mixed sample. It could be distinguished that the very small absorption coefficient difference of water between 0.004 at 660 nm and 0.01 at 785 nm by the system. 10 mg/dl concentration difference of black ink solution could be tell too. Moreover, its function could be enhanced to test three or more samples by adopting three or more optical wavelengths according to PA Lambert-Beer law. In this chapter, we only tried two kinds of ink solutions as sample. More samples (liquid, semisolid, solid, tissues) should be tested to optimize this PA system and enhance its measurement ability and

application range. In spite of the limited samples, the results clearly show the availability of this system. It could measure liquid, solid, even gas.

Furthermore, this prototype may work as a noninvasive and immediate spectrograph and apply to concentration measurement of key parameters in human tissue (oxyhemoglobin saturation, glucose etc.). It can work as wearable daily health diagnosis machine for home health care, or performance evaluation and control of exercise intensity in sport training. Moreover, optical spectrophotometer is a conventional equipment for optical absorption spectrum measurement. This prototype may work as PA spectrophotometer, which could enhance the sensitivity, capability and application range of electromagnetic spectroscopy.

In the next chapter, we will apply this system for PA contrast agent evaluation.

Chapter 3

Photoacoustic contrast agent evaluation by proposed compact photoacoustic system

In the past 30 years, first generation of photoacoustic tomography (PAT) mainly adopt human elements as target absorber, for example DNA, RNA, hemoglobin and lipid [74-75]. Recently, second generation of PAT tries to adopt exogenous contrast agent with high optical-absorption to enhance the performance of PA system. PA contrast agent is a hot research topic now [76-77]. By adopting PA contrast agent, it can greatly improve contrast, resolution and imaging depth of images. Moreover, it can provide additional functionality and extend PA tomography from genetic to whole human body imaging, and also revolutionize the diagnosis and treatment for living biological structures.

There are no suitable PA system now for contrast evaluation. Currently, major PAT implementations adopts nanosecond pulse laser and megahertz ultrasonic transducer. These equipment are expensive and huge, but not suitable for contrast agent evaluation. The PA spectroscopy system for gas, aerosol and process analysis also cannot meet this demand. A cheap and portable equipment is needed for preliminary evaluation of contrast agent. The key for contrast agent evaluation is to know optical absorption and PA signal from measured target.

In this chapter, in order to expedite the development of PA contrast agent, we use the portable PA system introduced in chapter 2 for sensitivity evaluation of PA contrast agent. The system adopts dual laser diodes operated with modulated continuous waves and a MEMS microphone at kilohertz region to make it compact, light and cheap.Some conventional and

new designed contrast agents were tested by this proposed setup.

3.1 Introduction of photoacoustic contrast agent

Contrast agent (also called contrast medium) is the materials used to improve the performance of biomedical imaging. It could enhance, for example, the contrast and spatial resolution of imaging for fluids or structures inside the body. Conventionally, we use it to boost the visibility of gastrointestinal tract or blood vessels by drinking or injecting contrast agent into body. Different kinds of contrast agents have been developed for different medical imaging and we could approximately classify them according to the adopted imaging modalities. In hospital, most common contrast agents work for X-ray CT and magnetic resonance imaging (MRI).

Now three main kinds of photoacoustic (PA) contrast agent have been developed for PAT: nano material, protein and fluorescence. Some research papers about nano material as PA contrast agent have been published, for example gold nanoparticle [78-79]. The size of nano material range from 10 to 100 nm and it could provide excellent imaging effect. By now, there is no clinic application of these nano materials. Protein is another choice of PA contrast agent, for example near-infrared fluorescent protein (IRFP) [80]. Normally the size of protein is smaller than 5 nm. It has poor imaging effect and did not be used in clinic. Fluorescence has been tried too [81]. One common example is indocyanine green (ICG). The size of fluorescence is much smaller, only less than 0.5 nm. It has been applied in clinic, unfortunately its imaging effect is also poor.

3.2 Measurement of ICG solution

Indocyanine green (ICG) is a fluorescence dye for video angiography used in medical imaging and diagnostics. Here, the photoacoustic capability of ICG solutions were measured by the proposed photoacoustic evaluation system introduced in chapter 2. ICG solution

consist of contrast agent ICG and solvent DMSO. DMSO has low and similar absorption at the two working wavelengths. It means the PA signal mainly results from the absorption of ICG.

3.2.1 Measurement of dimethyl sulfoxide (DMSO)

Dimethyl sulfoxide (DMSO) is an important and conventional polar aprotic solvent. All contrast agents tested in this chapter were mixed with DMSO to work as sample solution. This colorless liquid is an organosulfur compound, and is miscible in water and many organic solvents. Both nonpolar and polar compounds could be dissolved in DMSO. Absorptions of DMSO at 660 and 785 nm wavelengths are low and similar. Here we used experimental setup as Fig. 2.2 to measure DMSO. The working wavelength of laser here is 660 nm and average optical power is 20 mW. As shown in Fig. 3.1, PA signals of DMSO were always small and just reached the noise level (40-80 μV) of system, although we adjusted the modulated frequency from low to high. This measurement result meet the low absorption of DMSO and we could expect similar result with 785 nm laser.

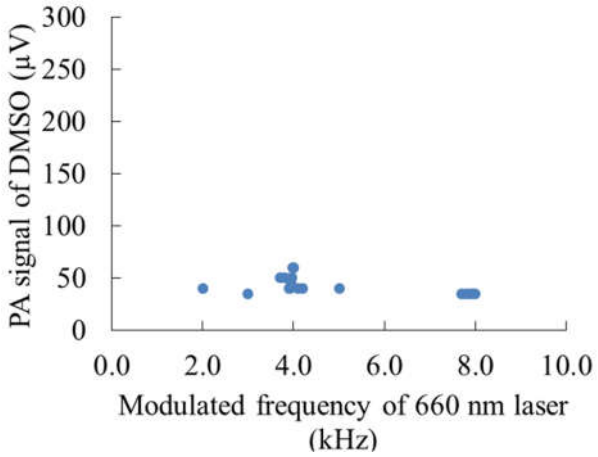

Fig. 3.1 PA signals of DMSO vs. modulated frequency.

3.2.2 Thermal diffusion length of ICG solution

As introduced in chapter 2, thermal diffusion length of sample is one of the key factor for sample measurement. In order to guarantee PA signal meeting equation (2.7), we should guarantee the sample length and optical absorption length are longer than thermal diffusion length of sample. Here we confirm this parameter for coming ICG solution experiment using the same PA system. The working laser wavelength is 785 nm and average optical power is 40 mW for this experiment. We prepared an ICG solution with concentration 17 μmol/L by mixing ICG and DMSO in a small dish. The diameter of dish is 20 mm. Fig. 3.2 shows the picture of ICG solution measurement. As shown in Fig. 3.3, the PA signals were stable when the height of ICG solution was reduced from 6 to 4 and 3.2 mm. Moreover, we could see the laser penetrate the whole sample solution by putting an infrared radiation detector card under the bottom of dish (Thorlabs, VRC5, IR Detector Card, 700 - 1400 nm). Thus we know the sample length and optical absorption length are long than thermal diffusion length of sample. Thermal diffusion length of sample should be longer than or same as 3.2 mm. If we change the concentration of sample, the thermal diffusion length should be also longer than or same as 3.2 mm, because the quantity of ICG is much smaller than DMSO. If we measure the sample by 660 nm laser, the result should be the same. Because thermal diffusion length will not change by wavelength and 660 nm laser can penetrate the whole sample. We didn't continue to reduce the length of sample for further confirmation because, in practical situation, it is difficult to measure when sample length is too short. Moreover, sample with 3.2 mm length is an appropriate volume and normally easy to prepare.

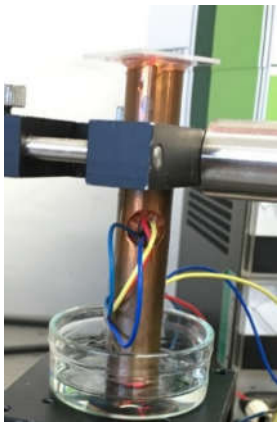

Fig. 3.2 measurement picture of ICG solution.

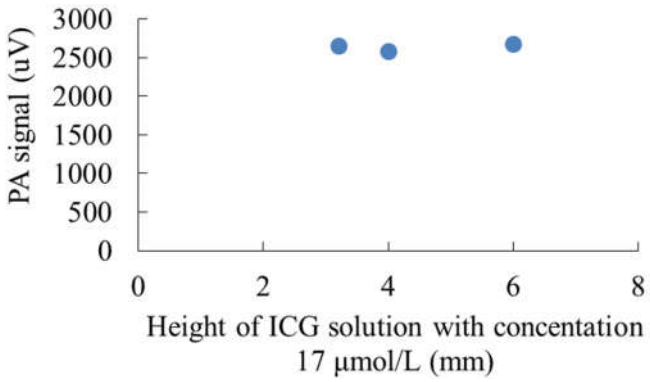

Fig. 3.3 PA signals vs. height of ICG solution.

3.2.3 PA signal vs. concentration of ICG solution

Here we prepared a 4 ml ICG solution with 4 mm depth in the same dish. We recorded the PA signal by the change of solution concentration using LD with 660 and 785 nm wavelengths. According to Fig. 3.4, the absorption of ICG at 785 nm shifts from the peak wavelength (800 nm), but still strong, while absorption at 660 nm is only about 15% of 785 nm. As shown in Fig. 3.5, the PA signal increased almost linearly with the increase of ICG solution concentration at 785 nm. This system is sensitive and can distinguish small

concentration difference (2.5 μmol/L) of ICG solution. But higher concentrations have some unexpected responses, which may result from the instability of the sample. During the measurement, the averaged optical power of 785 nm laser is around 40 mW. This high-power and focused laser may lead to the thermal and opto-active effects on ICG solution. This is one possibility of sample instability. While 660 nm, although we increased the concentration of ICG solution to 80 μmol/L, or even 640 μmol/L, the PA signals kept the same as noise level (80 μV), shown as Fig. 3.6. That is because the absorption of ICG at 660 nm is much smaller and the average optical power is 20 mW, only half of that at 785 nm.

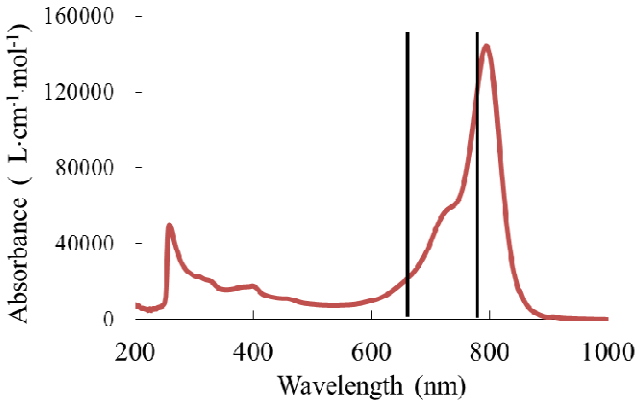

Fig. 3.4 Absorption of ICG.

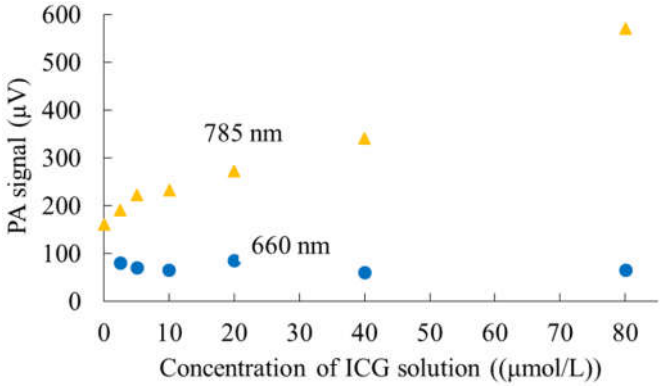

Fig. 3.5 PA signal level as a function of concentration of ICG solution.

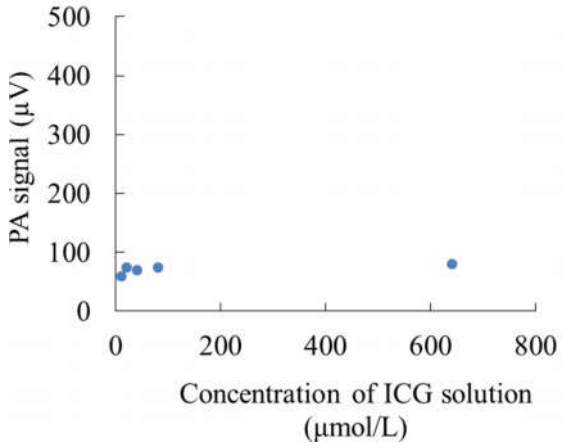

Fig. 3.6 PA signal level at 660 nm as a function of concentration of ICG solution.

3.3 Measurement of TO-001, TO-002 and TO-003 solution

Here we use same system to measure TO-001, TO-002 and TO-003 solution, which consists of contrast agent TO-001 (or TO-002, TO-003) and solvent DMSO respectively. TO-001, TO-002 and TO-003 compounds are organic (non-metal) dyes.

Working wavelength is 785 nm and average optical power is 40 mW. Firstly, TO-001 solution with 20 μmol/L concentration was prepared and exposed to 785 nm lase. We found the color of solution change obviously from original light green to brown, and even black in one minute. Since sample TO-001 is unstable, and have strong optical absorption at wavelength 785 nm. This high absorption at 785 nm laser accelerated the instability.

Then, we prepared another TO-001 solution with 80 μmol/L concentration. To increase the concentration, we want to see longer reaction period and roughly confirm the absorption of contrast agent TO-001. When this solution was exposed to laser, again the color of solution changed gradually from original light green to brown, and even black. It is same as last measurement, but the time period is longer. At the same time, we could detect obvious PA signal, and see the signal decreased gradually by testing time, as shown in Fig. 3.7. The PA signal decreased by 17% in 5 minutes.

The measured PA signals met the phenomenon we observed, which imply the sensitivity

of PA system. When exposing the solution to laser, the change of material structure leads to the change of color, and finally reduced the absorption ability of TO-001. Moreover, by increasing the concentration of sample, the reaction period was slow down. Because the TO-001 on solution surface reacted with laser first, then the parts inside the solution reacted.

TO-002 and TO-003 were also measured at 785 nm, but both PA signals were weaker than TO-001 due to their lower optical absorption at 785 nm. The average PA signals of TO-002 and TO-003 at 80 μmol/L were 410 and 320 μV respectively in first three minutes, but they were also unstable

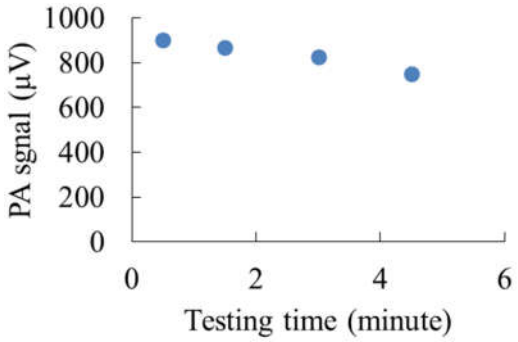

Fig. 3.7 PA signal of TO-001 at 785 nm vs. testing time.

3.4 Measurement of carbon powder

Here we have designed a new method, as shown in Fig. 3.8, to test sample with small volume by this PA system, at the same time this method could be used to measure powder material which may be future contrast agent candidate.

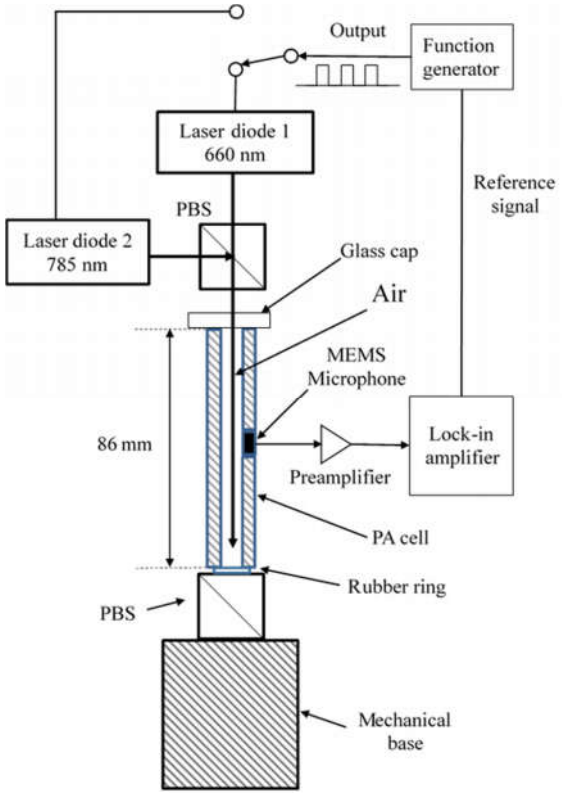

Fig. 3.8 Measurement of carbon powder.

We adopt a cubic PBS (polarization beam splitter, dimension: 20 X 20 X 20 mm) as base to put sample. The reason we adopt polarization beam splitter is the laser beam will not be reflected back after penetrate the sample. Then a rubber ring (external diameter: 9 mm; internal diameter: 6 mm;) was put on the surface of PBS. The rubber ring help to seal the PA cell. After that, we put the sample we want to test, ink drop or carbon powder, inside this ring. Fig. 3.9 show the pictures of powder and ink drop measurement .

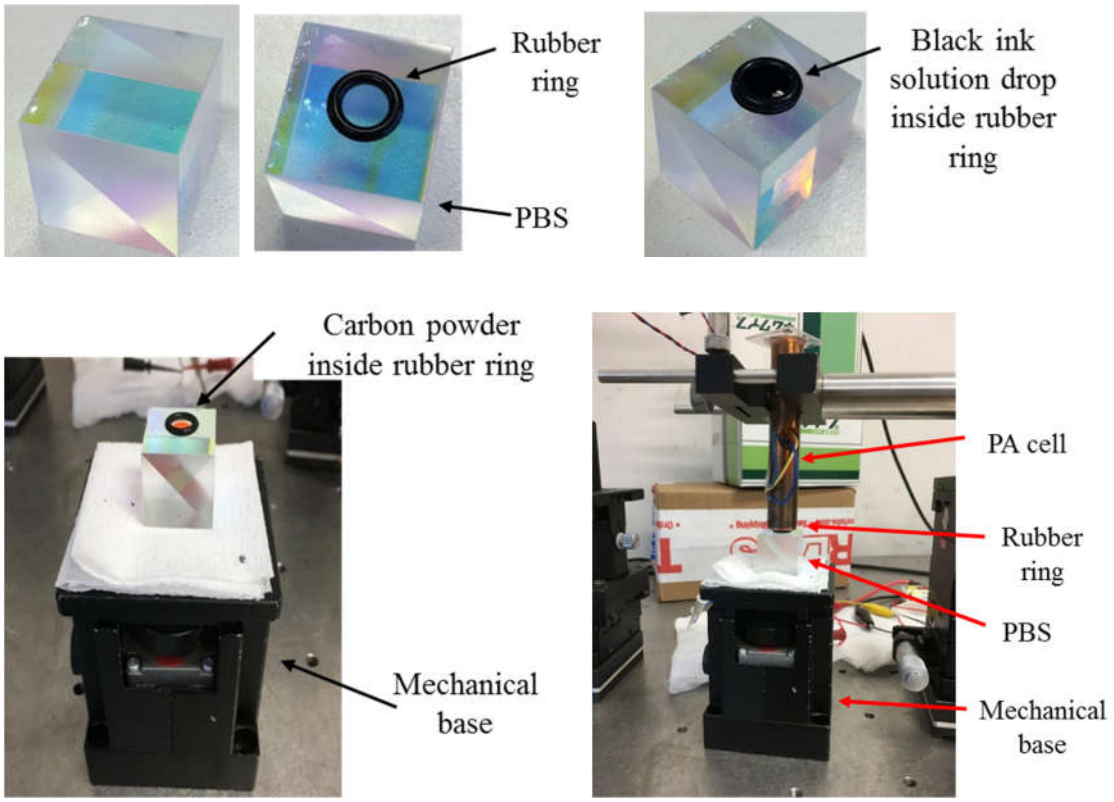

Fig. 3.9 Pictures of powder and ink drop measurement .

Fig. 3.10 shows the measurement results of ink drop and carbon powder at 660 and 785 nm. The yellow points here represent PA signals of powder at 785 nm, while blue points represent PA signals at 660 nm. Black points represent PA signals of ink at 785 nm. We found clear PA signal peaks of powder and ink at 785 nm when frequency is around 4 and 8 kHz. It means this new measurement way works and powder has strong absorption at 785 nm. While at 660 nm, PA signals of powder is always small no matter what frequency is. It means this powder has small absorption at 660 nm.

By now, we found a new method to test sample with small volume by this PA system. Moreover, we know this PA system could be used for liquid, solid and powder testing.

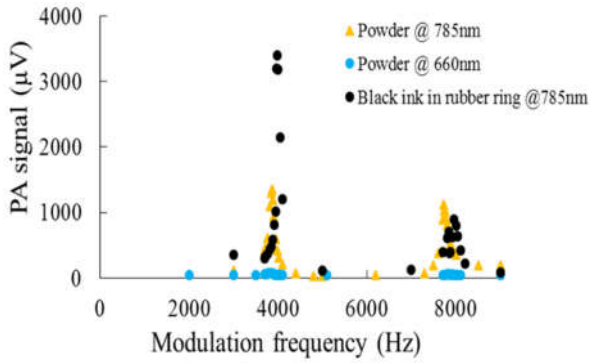

Fig. 3.10 Measurement result of powder and ink drop.

3.5 Noises affect PA measurements

Here we want to confirm how noise affect PA measurement. An ICG solution with 20 μmol/L concentration was prepared. The height of sample is 4 mm and the volume is 4 mL. Working laser here is 660 nm with 20-mW average optical power.

We changed the modulation frequency gradually and found the first and second peak PA signal were 285 and 175 μV respectively at 4.04 and 8.06 kHz. Then someone spoke loudly in the experiment room and the peak PA signals disappeared. The results were shown in Fig. 3.11. The PA signals were low and strange because noise level was high enough to affect the PA signal and the resonance inside PA cell. This phenomenon happened when measuring ink solutions. Loud voice, high sound of closing door or other noises have the same effect. Moreover, the noise obviously affected the measurement results especially when the depth of sample is shallow and the size is small. We guess PA signal failed to be resonated and amplified inside PA cell when noise is high. When the size of sample is large and height is long, impedance difference between air inside PA cell and its borders is high. It becomes easy to form resonance inside PA cell and difficult for noise to penetrate sample and affect the PA signal.

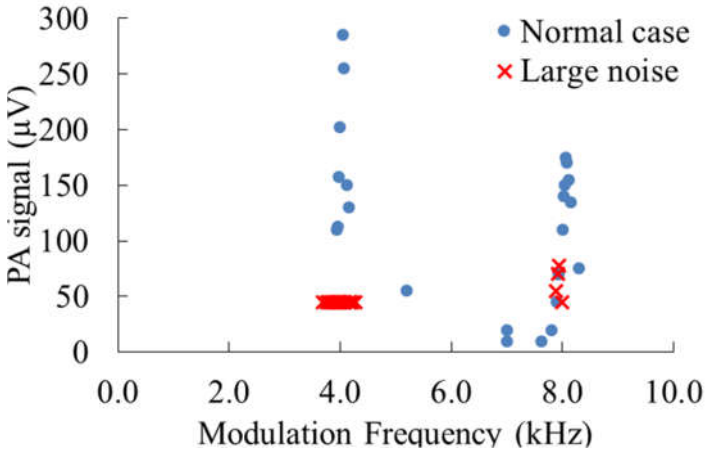

Fig. 3.11 PA signal affected by background noise.

3.6 A strange phenomenon with high concentration solution measurement

When we measured high concentration solution, no matter ink solution or ICG solution, sometimes there was a strange phenomenon happening sometimes. As shown in Fig. 3.12, PA signal increased with testing time when ICG solution with high-concentration 80 μmol/L. At the beginning of measurement, the PA signal was 570 μV. Then it gradually increased to 645 and 725 μV at third and sixth minute. After that, the signal basically kept stable and reached 750 μV at sixteenth minute. The working wavelength of laser is 785 nm with 40 mW average optical power. The same phenomenon happened when the sample was high-concentration black ink. At that time, PA signal increased gradually with time and finally have been doubled. The increase of PA signal lasted for 30 minutes and finally became stable.

It is possible that high-concentration sample strongly absorbed laser power, which resulted in accumulating heat. These heat finally changed the temperature of sample and leaded to the instability of sample. Furthermore, the temperature and humidity of air inside PA cell were changed by these accumulated heat. Part of sample may volatilize into the air inside PA cell and changed the concentration and constituents of air. The volatilized sample would absorbed laser and generated PA signal too. All these mentioned factors can affect the

detected PA signal. PA system is a complicated design and many factors may affect the PA signal. However, when the stability of external conditions are guaranteed and measurement range of sample are suitable, this PA system is reliable and sensitive.

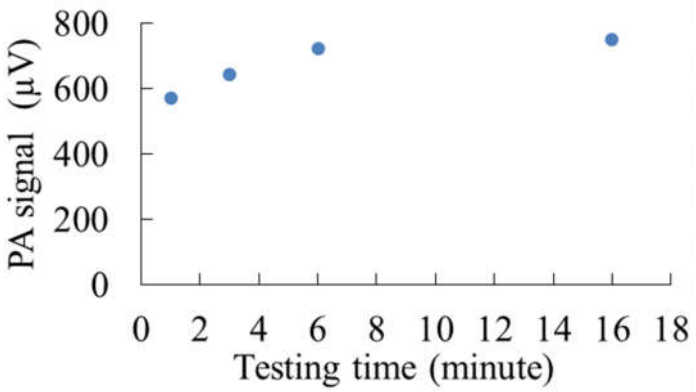

Fig. 3.12 PA signal vs. testing time.

3.7 Future work

In order to develop new PA contrast agent, we have a research team in our university. Fig. 3.13 shows the research team and functions. Firstly, several material groups will design new materials for contrast agents. Our group will design PA system to evaluate these contrast agents. Then biology group will apply these contrast agents for living animals for in vivo test. In the future, we hope to cooperate with company to use these contrast agents for PA imaging and diagnosis in clinic applications. The contrast agents we tested in this chapter were developed by those material groups.

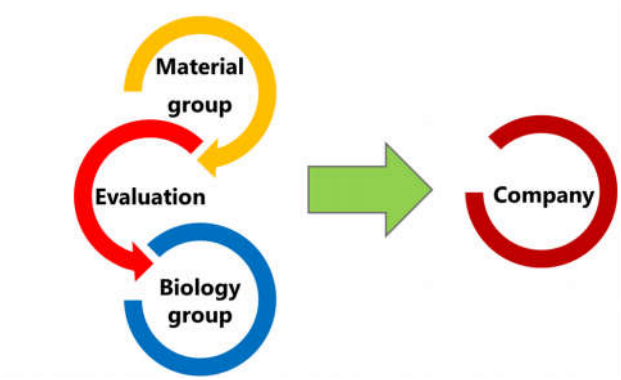

Fig. 3.13 Research team and functions

Conventionally, we adopt light source and contrast agent working in the range of 600-1000nm. Here, the target of our research team is to develop PA contrast agents working at 1310nm, which can avoid primary biological absorbers from human tissue, such as hemoglobin, melanin and water. By this way, the absorption loss from tissue becomes much less. Fig. 3.14 shows the optical windows in human body [82]. Moreover, 1310nm is a common wavelength in telecom. There are various optical and electronic equipment and tools available for different application demands. We can adopt these equipment to make system smaller, lighter and cheaper.

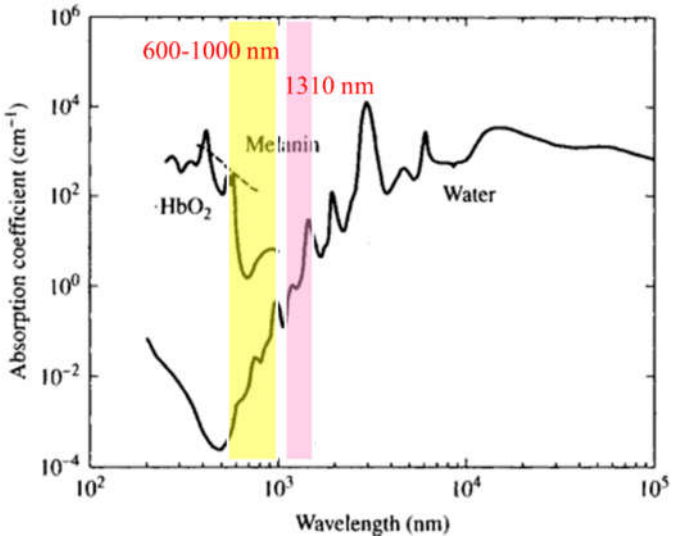

Fig. 3.14 Primary biological absorbers of human tissue.

In chapter 2 and this chapter, we adopt laser working at low frequency (kHz). In the future, we plan to develop PA system working at high frequency (MHz). MHz is conventional working frequency for PA tomography system. By combining the measurement result of kHz and MHz, we could understand the PA contrast agent comprehensively. Fig. 3.15 shows the design of MHz PA system for PA contrast agent evaluation working at 1310 nm wavelength. A tunable laser working at around 1310 nm is modulated by a function generator to provide MHz rectangular optical signals. A MHz ultrasonic transducer is adopted as ultrasonic detector. A cell with 30 mm height and 10 mm width works as sample container. Finally, preamplifier and lock-in amplifier are used to process the measurement results.

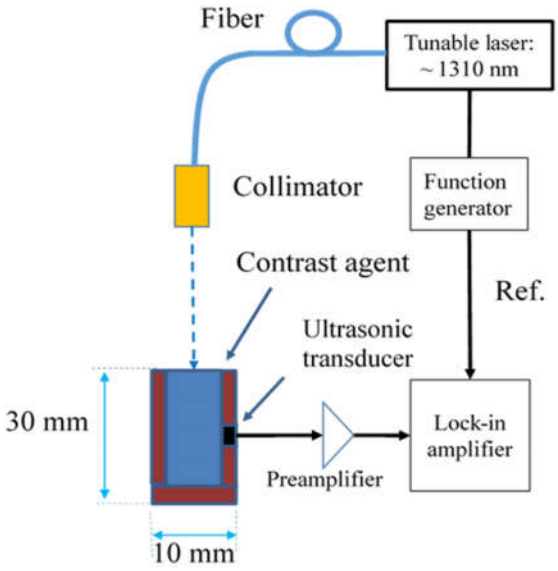

Fig. 3.15 MHz PA system design.

3.8 Conclusions

Photoacoustic tomography (PAT) adopts contrast agent for better images and more functionality. In this chapter, the compact PA system proposed in chapter 2 is applied to evaluate PA contrast agents. The sensitivity of the PA system was successfully confirmed by

PA contrast agent evaluation, including ICG solution, TO-001, TO-002 and TO-003 solution. This system can distinguish 2.5 μmol/L concentration change of ICG solution at 785 nm. It could work as a convenient equipment for contrast agent evaluation in PAT.

Moreover, a new method to test sample with small volume by this PA system has been found. We confirm this PA system could be used for liquid, solid and powder testing.

In near future, we should compare the measurement results from this PA system and PA image detected by commercial PA imaging equipment. We hope the development of new exogenous PA contrast agent could be accelerated by this proposed PA system. It will help new generation of PA imaging for medical applications.

Chapter 4.

Sound intensity measurement for ultrasound under water using light emitting diodes and piezoelectric elements

Photoacoustics consist of two parts: optical excitation and acoustic detection. Here we provide a novel acoustic detector, which could be used for photoacoustic and other related acoustic applications. Sound pressure and sound intensity distribution was measured to confirm this new acoustic detector.

4.1 Working principles of LED-PZT sensor

4.1.1 Configuration of LED-PZT sensor

Fig. 4.1 shows the configuration of single LED-PZT sensor. A visible-light light emitting diode (LED) is connected to the electrodes of a cylindrical piezoelectric (PZT) element (diameter = 5 mm and height = 10 mm). The material of the piezoelectric element is lead zirconate titanate ceramics, and it is polarized in the direction of its axial. Its top and bottom surfaces have thin silver layers for electrodes, which connect to the leads of LED.

LED was polished and make the luminous surface flat, which is convenient to connect with plastic optical fiber (POF). A cap fixes POF to LED firmly. DC power supply provides DC voltage for LED by a 10 nF capacitor and a 330 Ω resistor.

Fig. 4.2 shows the working principle of LED-PZT sensor. The LED works at the linear range by controlling DC power supply. When PZT element detecting an ultrasonic signal, the sound pressure fluctuation induces a dynamic AC voltage passing PZT element, then leads to the fluctuation of LED current and the change of optical signal. This optical signal is measured by a photodetector located at a far place through POF (1 mm diameter). Finally, optical power fluctuation of LED is proportional to the magnitude of sound pressure. By this way, we can confirm the acoustic signals by the optical signals of LED.

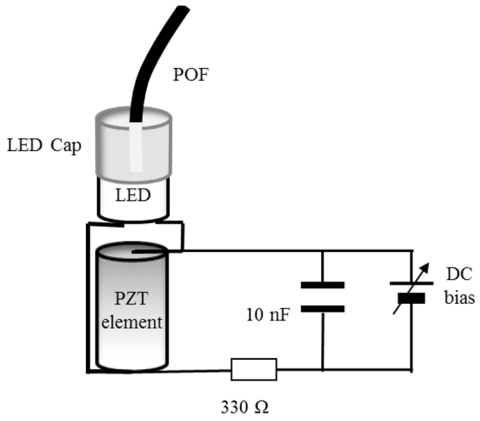

Fig. 4.1 Configuration of single LED-PZT sensor.

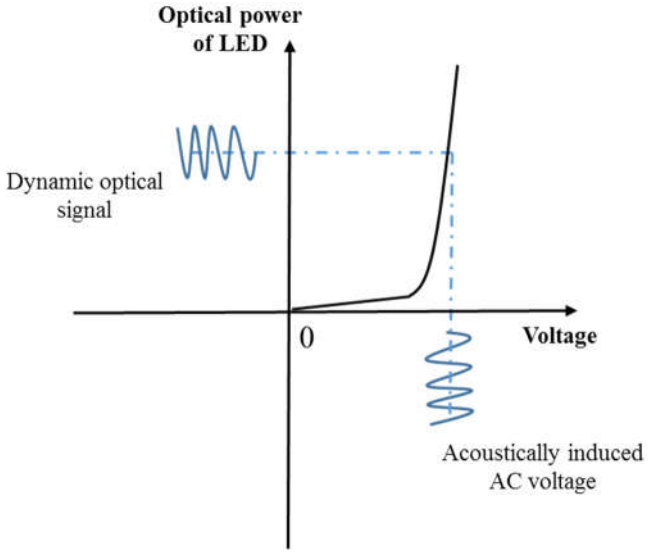

Fig. 4.2 Fundamental of LED-PZT sensor.

4.1.2 Process to make LED-PZT sensor

There are several processes should care when making sensor. Fig. 4.3 shows the PZT element, LED and polished LED. Fig. 4.4 and 4.5 show the hand-made LED-PZT sensor used in experiments.

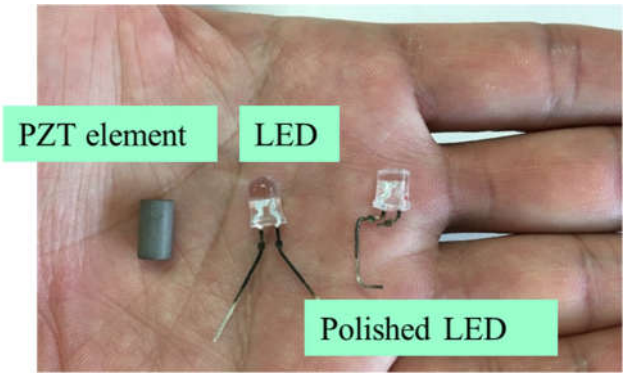

Fig. 4.3 Pictures of PZT element, LED and polished LED.

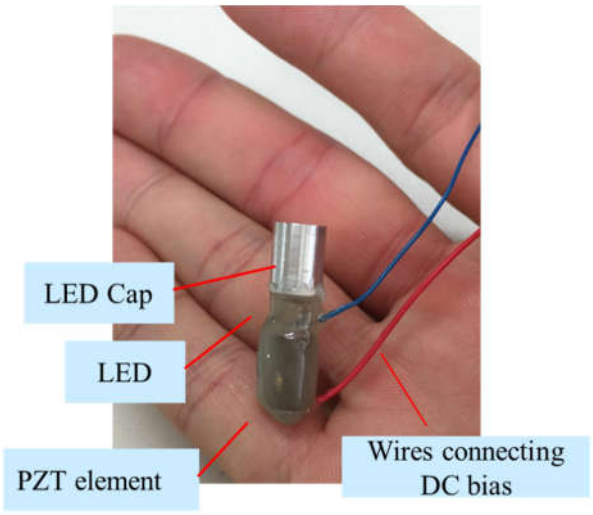

Fig. 4.4 Pictures of LED-PZT sensor.

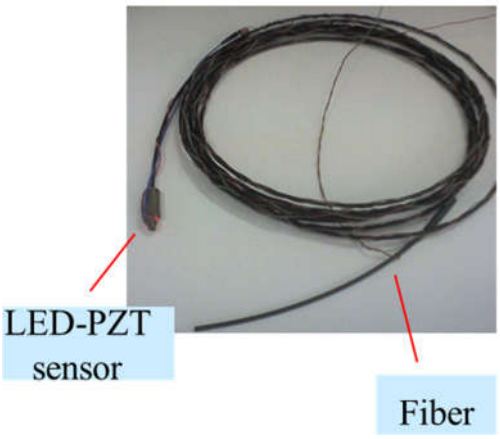

Fig. 4.5 Picture of LED-PZT sensor with fiber.

The LEDs were polished by file and fiber-polishing film respectively. Firstly, luminous surfaces of LEDs were polished from sphere to flat by file for easily fixing fiber. The distance between LED chip and luminous surfaces should be polished properly. The distance is too far will make the light from LEDs weak, while too close will make the light too strong and may damage the circuit of LEDs. Then we used different grades of fiber-polishing film for successive polishing cycles (THORLABS, Fiber Polishing/Lapping Film, grit sizes of 30, 6, 3 μm) to control the output light precisely. A

finer grit paper was used for each polishing cycle. The ends of fiber were polished in the same way too. But the surfaces of fibers were not polished flat. We tried to keep it had small angle, around 8 °, for smallest insertion loss and highest return loss. Big return loss may affect shining of LEDs.

After polishing, LED is soldered to the electrodes of piezoelectric element. While soldering, we should pay attention to the heating temperature which may damage LED and PZT element. Moreover, we tried our best to make the direction of piezoelectric element and LED straightly, to make the whole LED-PZT sensor look cylindrical, as shown in Fig. 4.4. This uniformity of all sensors help to control the measurement precision for not only single LED-PZT sensor but also multi-channel sensor array while sensors are fixed to mounting bracket. If the PZT element is slanting from the direction of LED, different sensors will have measurement error which will result in the error of amplitude and phase.

After soldering, the LED and piezoelectric element were covered by glue (CircuitWorks, Conductive Epoxy CW2400) for waterproofing and protection. The glue coating doesn’t affect the measurement result because the acoustic wavelength is much longer than the thickness of glue coating. We try to make the glue coating thin and uniform for less transmitting loss and higher sensitivity. Moreover, there should not have air layer between PZT element and glue coating which will seriously reduce the sensitivity of sensors. Big bubble in the glue coating should be avoided too, which increase the impedance and affect the sensitivity of sensor.

4.2 Characteristics of LED-PZT sensor

4.2.1 Signal delay of LED-PZT sensor

Signal delay is another key factor we should consider for this research. We prepare the setup as Fig.4.6 to compare the referenced signal from function generator and optical signals of four colors LED from photo detector (PD). Fig.4.7 shows the picture of the setup. The optical signal of LED was modulated by a function generator and controlled by a 330Ω resistor. Optical signal was detected by PD then analyzed by oscilloscope. Finally we compare the optical signal from LED with referenced signal from function generator to know the time delay between them. When measuring the optical signal from LED, we should choose proper distance between LED and PD to make sure the optical power is not out of PD measurement range. As shown in Fig.4.8, four colors LEDs have same time dely. There will be 2 μs time delay when modulation frequency started from 10 kHz. The time delay kept the same when modulation frequency increased up to 200 kHz. As we know, the responding time of LED, the PZT element and photodiode inside photo detector is ＜1 us, ~1 us and ~0.01 us respectively, which is much quicker than 0.1 ms (corresponding modulation frequency 10 kHz). The time delay should result from the electric signal processing inside photo detector. In this research, we just need to compare the phase difference between different sensors. This time delay will not affect the measurement result finally because all color LED and sensors have same time delay. Moreover, the time delay could be removed when better PD is used.

Moreover, the frequency response of photo detector will affect the signal delay too. We should set all photo detectors at same frequency response. We also did experiments

to confirm other factors will not affect signal delay, for example DC voltage of LED, optical coupling between fiber and LED.

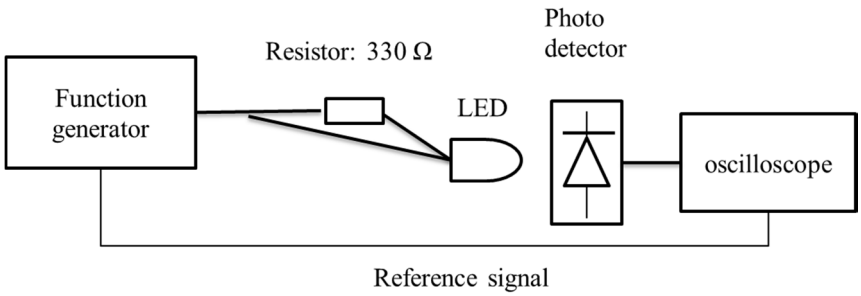

Fig. 4.6 Experimental setup to confirm signal delay.

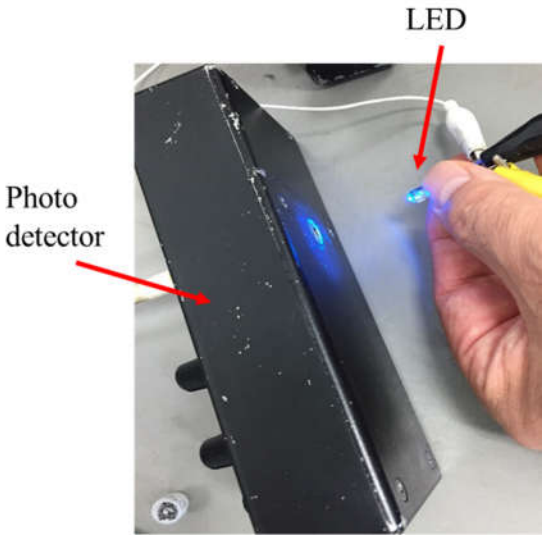

Fig. 4.7 Picture of experimental setup to confirm signal delay.

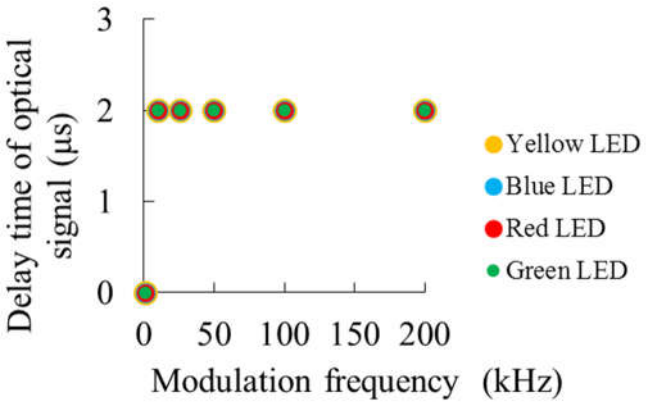

Fig. 4.8 Delay time of optical signal when changing modulation frequency.

4.2.2 Optical signals vs. DC voltage of four LED-PZT sensors

We use the measurement system of single LED-PZT sensor, as shown in Fig. 4.9, to understand the relationship between optical signals and DC bias of four sensors. Fig. 4.10 shows the results. This testing result meets the curve of Fig. 4.2, and all sensors' optical power is linear with DC bias when DC voltage ranging from about 2 to 4 voltage, as shown in Fig. 4.10 (a). Here all sensors' slope shown in Fig. 4.10 (b) at the linear part are similar to each other, about 3.8. The slope represents the sensitivity of sensors. As shown in Fig. 4.2, when the slope is higher, the AC voltage induced by acoustic signal leads to higher optical power of sensor. In this research, we should carefully keep slopes of all sensors very similar to each other to guarantee all sensors have similar sensitivity to AC signal. This is one of the key of this design.

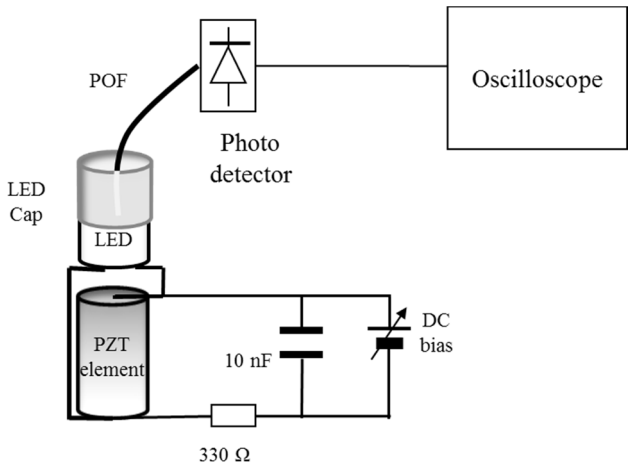

Fig. 4.9 Measurement system of single LED-PZT sensor.

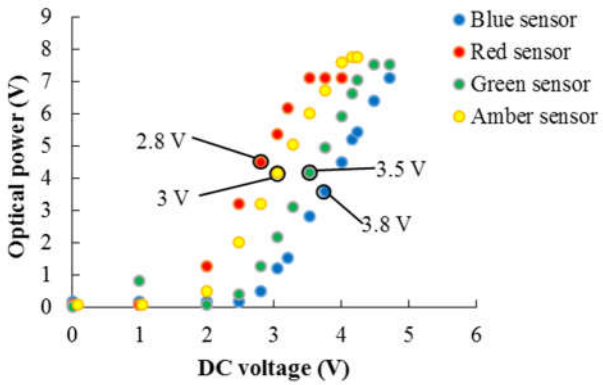

(a)

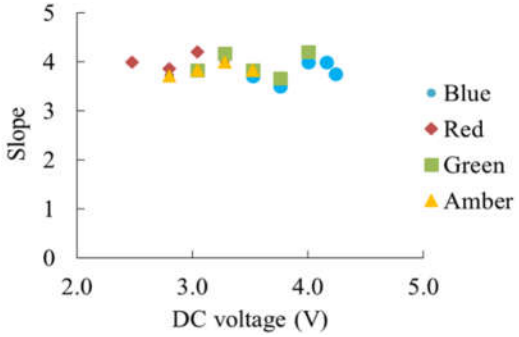

(b)

Fig. 4.10 Optical signals vs. DC voltage of four LED-PZT sensors. (a) Optical power vs. DC voltage of four LED-PZT sensors; (b) Slope of optical signals vs. DC voltage of four LED-PZT sensors.

In order to guarantee all optical signals fall at around the middle of measurement range of photodetectors and four sensors have same sensitivity, we set the DC voltage of LEDs falling in this linear part. The working DC voltages of red, amber, green and blue LED are 2.8, 3, 3.5 and 3.8 V respectively. When detecting same acoustic signal, different-colored sensors generated equal AC voltages and the optical power of sensors changed correspondingly. By calibration, we can determine the acoustic signals finally. This is the key working principle of this research.

Fig. 4.11 shows the sensitivity of each sensor, where the sound pressure was tested by a conventional hydrophone (Brüel & Kjær, 8103) and compared with the four LED-PZT sensors. Good linearity is shown up to 10 kPa range. The differences among the outputs might be caused by the difference in the waterproof coating of the PZT elements and the variation in the optical coupling between the LED and the fiber.

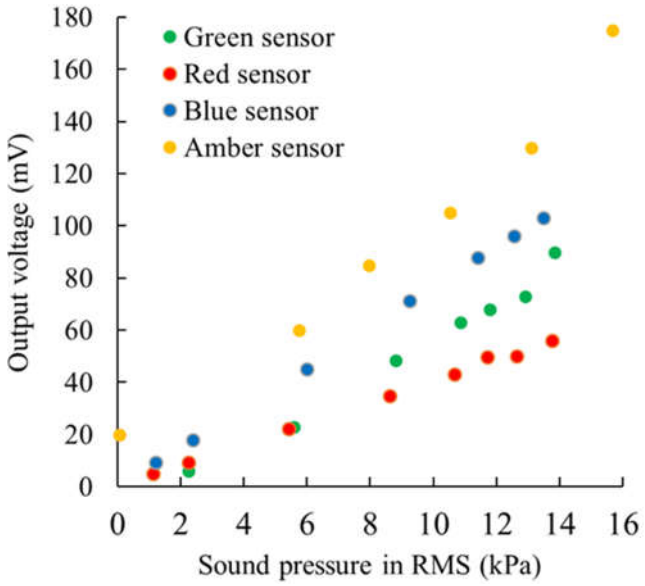

Fig. 4.11 Output voltages of sensors vs. applied sound pressure.

In order to choose suitable and similar sensitivity and slope for sensors, there are several processing factors should be considered. Firstly, we polished two ends of plastic optical fiber (POF) in Fig. 4.9 to change the percentage of LED light coupled to measurement system. As shown in Fig. 4.12, the slope of optical signals increase when the fiber is polished better and more light is coupled into PD. By this way, the sensitivity of sensors increase. Secondly, the slope increase with the gain of PD, as shown in Fig. 4.13. However, it doesn't mean higher slope is better. When the gain of PD or the coupled light is too high, the optical power will be out of the measurement range of PD. To polish the fiber and choose gain of PD properly is one of the key for sensor design. In this research, the optical power ratio between DC voltage and AC voltage from acoustic signal is around 1000 times for four-color sensors, which guarantee the sensitivity of sensors.

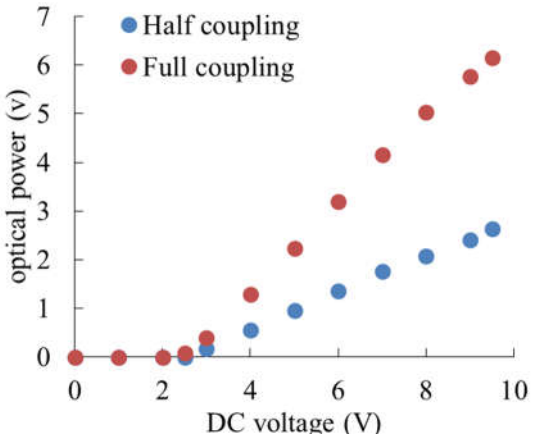

Fig. 4.12 Slope of sensor' optical signals vs. coupled light.

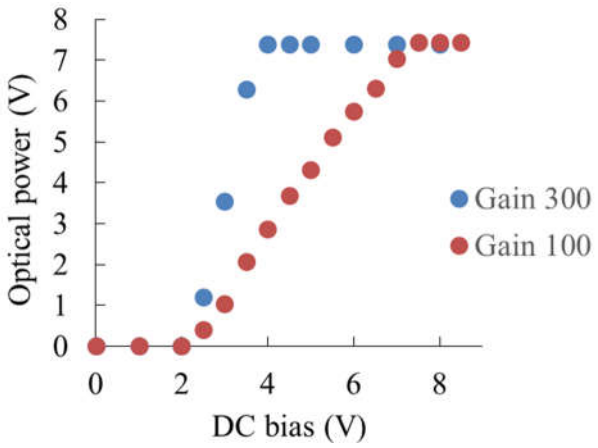

Fig. 4.13 Slope of sensor' optical signals vs. gain of PD.

Moreover, the sensors were fixed to mounting bracket on LED cap. We should pay attention to the fixing pressure. If the pressure is too strong, it will change the shape of LED cap and the percentage of coupled light, then change the slope and sensitivity of sensors. If the pressure is too light, the position to fix is not stable, then the measurements error will be high.

4.2.3 LED-PZT sensor test in 26 kHz ultrasound field

4.2.3.1 Measurement setup

The measurement setup and coordinate system are shown in Fig. 4.14. The signals from function generator were amplified by power amplifier, then input to transducer. An ultrasonic transducer worked at 26.35 kHz as sound source, which is driven by function generator and power amplifier. The blue part is water in tank with dimension 420 x 320 mm. The transducer is clamped at the wall of water tank and fixed by silica gel. Its front end was immersed in water. This transducer consists of a bolt-clamped Langevin transducer and a straight half-wavelength horn. The horn is mounted at the wall at its

node, and its circular radiation surface is 50 mm in diameter. The center of transducer is 65 mm away from the surface of water and 110 mm away from the bottom. Fig. 4.15 and 16 show the measurement setup without and with absorber respectively.

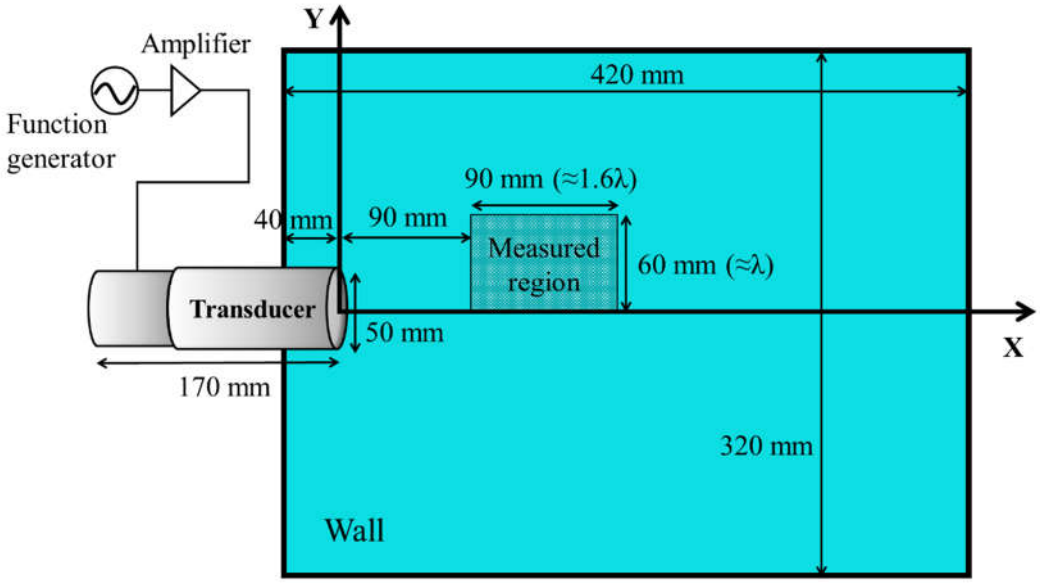

Fig. 4.14 Measurement setup and coordinate system.

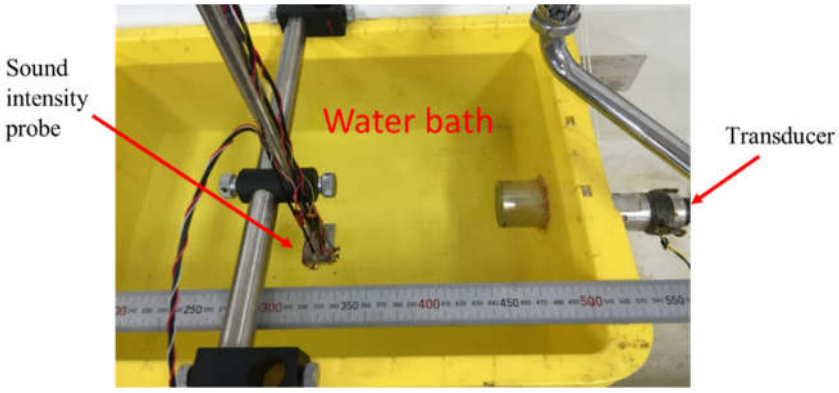

Fig. 4.15 Picture of measurement setup without absorber.

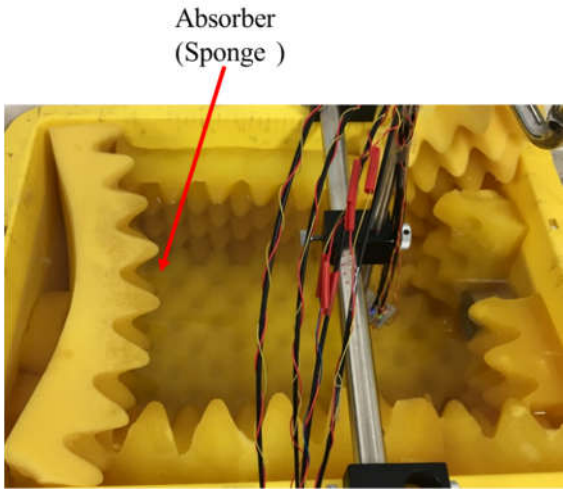

Fig. 4.16 Picture of measurement setup with absorber.

Before experiments, we reduced the noises of sensors by 10-20% by rearranging the equipment in proper places to reduce wires twining. We also replaced the metal screws to fix sensors by plastic ones, but noises changed little.

4.2.3.2 Sound pressure and phase test

We used a commercialized piezoelectric hydrophone (Brüel & Kjær, 8103) to scan along the x-axis of ultrasonic filed. The amplitude and phase of hydrophone changed gradually by position changing. Both traveling and standing wave patterns were observed. Then we use four-color LED-PZT sensors to scan the ultrasonic field in the same way and same characteristics wave pattern were observed from every LED-PZT sensor. It means, basically, these LED-PZT sensors can work as commercialized piezoelectric hydrophone.

For further confirmation and understand the linearity and accuracy of each LED-PZT sensors, we compare the sound pressure and phase from a commercialized piezoelectric hydrophone (Brüel & Kjær, 8103) with the four-color LED-PZT sensor. The

five sensors were fixed in a different position in the ultrasound field. Then we increased the current of transducer to increase its output power. As shown in Fig. 4.17 and 4.18, the amplitudes of five sensors increased almost linearly with the increase of transducer current and the phases of sensors kept similar. The maximum phase deviation of one sensor is around 0.5 radian, which may result from the fluctuation of transducer output. The characteristics of LED-PZT sensors are the same as commercialized piezoelectric hydrophone. Here, in principle, we confirmed the new designed sensors can work as commercialized piezoelectric hydrophone.

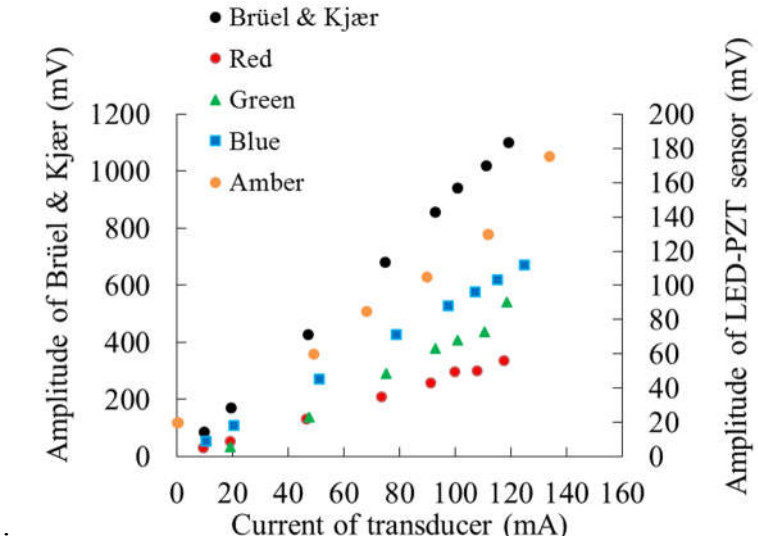

Fig. 4.17 Current of transducer vs. amplitude of BK and four LED-PZT sensors.

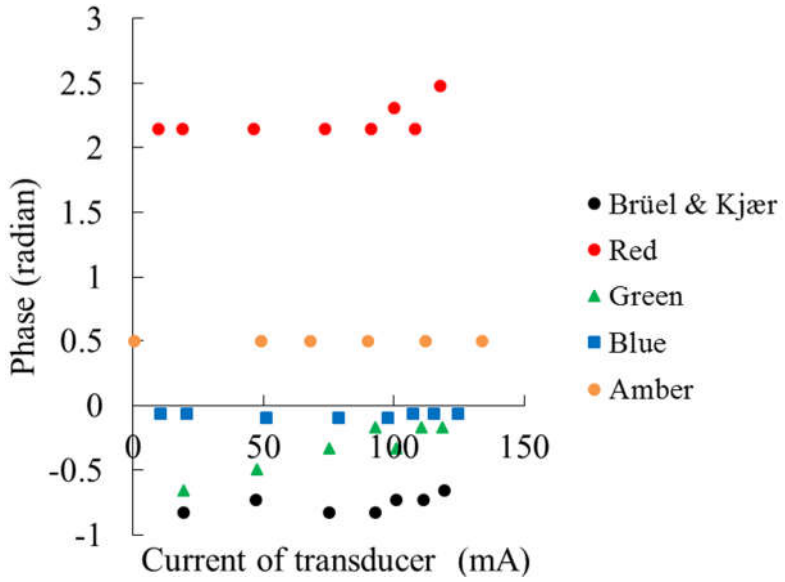

Fig. 4.18 Current of transducer vs. phase of BK and four LED-PZT sensors.

Here we explain how the Fig. 4.17 was produced. Form the output voltage of B&K sensor V and current of transducer I, we found the relationship

$$V = 9.2 \cdot I \,. \tag{4.1}$$

through the fitting by y=ax. V is the output voltage of B&K sensor (unit: mV) from oscilloscope, while I is the current (mA) of transducer. According to the B&K's spec, its sensitivity is 0.028 mV/Pa. Using this sensitivity, we can know the relationship between sound pressure measured by B&K sensor (Pa) and the current of the transducer:

$$P = \frac{V}{0.028} = 330 \cdot I \,. \tag{4.2}$$

Moreover, the voltage of all sensors we read from oscilloscope is peak-peak, we translate it to root mean square value (RMS)

$$P_{RMS} = \frac{P_{\text{peak-peak}}}{2\sqrt{2}} = \frac{P_{\text{peak-peak}}}{2.82} \,. \tag{4.3}$$

Because usually in sound industry, sound pressure are measured in RMS value. Moreover, sound intensity has been widely used in the area of noise where RMS has

been commonly used in sound pressure. But in some of ultrasonic research, sound pressure is measured in 0-peak value since the maximum pressure has sometimes important meaning in high power applications.

Then, according to equation (4.2) and (4.3), we have

$$P_{RMS} = \frac{330 \cdot I}{2.82} = 117 \cdot I \,, \tag{4.4}$$

The unit of P_{RMS} is Pa, while that of I is mA. Using equation (4.4), output voltages of four LED-PZT sensors were plotted as functions of sound pressure, as shown in Fig. 4.16. Here the voltage of B&K was measured as peak-to-peak value from the display of the oscilloscope, then calculated to RMS value.

In order to confirm the shape uniformity of single LED-PZT sensor, we put the sensors into the ultrasonic field and rotated them in a fixed position. The output amplitude and phase kept basically the same when rotating. It means the shape uniformity of single sensor is enough for this measurement.

4.2.4 LED-PZT sensor test in 38 kHz and 1.6 MHz ultrasound field

To further understand the performance of sensor, we tested the red LED-PZT sensor in 38 kHz and 1.6 MHz ultrasound filed respectively. Fig. 4.19 and 4.20 shows the experimental setup. The ultrasound source is an ultrasonic cleaner working at 38 kHz (株式会社エスエヌデイ US-2KS; Working frequency: 38 kHz; High frequency output: 120 W; Water tank dimension: 237×137×100 mm.). LED-PZT sensor was put into the water tank and scanned different position. When moving the sensor, only the PZT element of sensor is dipped into the. The water depth of ultrasonic field is 12 mm. The sensor head is around 2 mm from the bottom of water. As shown in Fig. 4.21, the amplitude of sound

pressure changed obviously by position changing. The detected frequency was always same as the working frequency of ultrasonic cleaner, 38 kHz, no matter which positions were. Positions 1-6 located in corners, borders and centers of ultrasonic cleaner respectively. We can also found when changing the dipping depth of PZT head, the amplitude changed too. It is because ultrasonic signals are different in different depth of field. The maximum amplitude is higher than three times of the minimum.

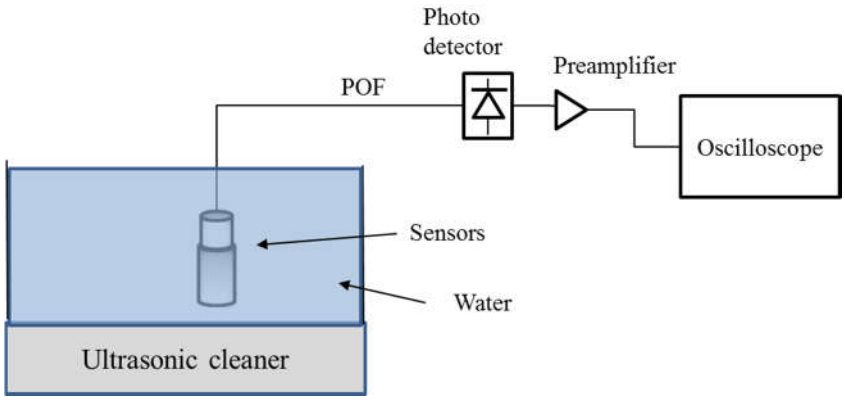

Fig. 4.19 Experimental setup of 38 kHz ultrasound field.

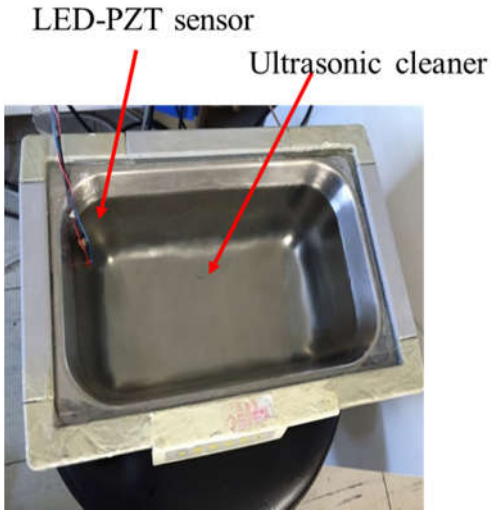

Fig. 4.20 Picture of experimental setup of 38 kHz ultrasound field.

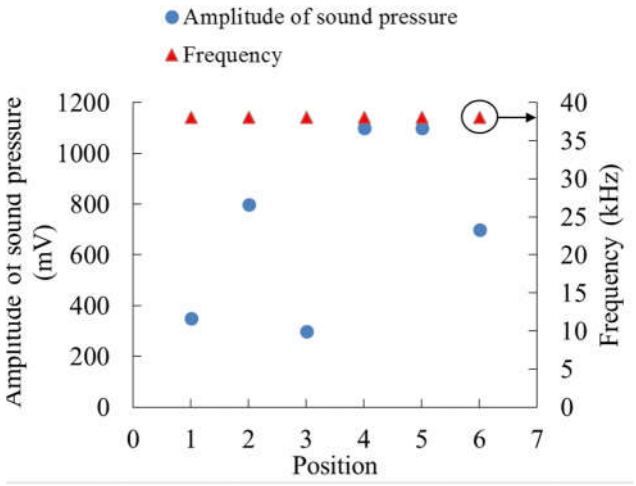

Fig. 4.21 Measured amplitude and frequency at different position by LED-PZT sensor

In the second experiment, we use this sensor to measure 1.6 MHz ultrasound field. Fig. 4.22 and 4.23 shows the experimental setup. An ultrasonic atomizer unit worked as ultrasound source to provide 1.6 MHz ultrasonic signal (HONDA ELECTRONICS HM-1630; Working frequency: 1.6 MHz; Current: 620 mA; Dimension of transducer: 42 x 30 x 11mm;). The ultrasonic output was so strong that the water surface near the transducer fluctuated. We used the red LED-PZT sensor to scan different position around the axis of ultrasonic output. As shown in Fig. 4.24, the amplitude of sound pressure changed obviously by different position. The detected frequency was always same as working frequency of the transducer, 1.6 MHz. When the sensor is more than 10 cm away from the axis of output, we cannot observe any signal.

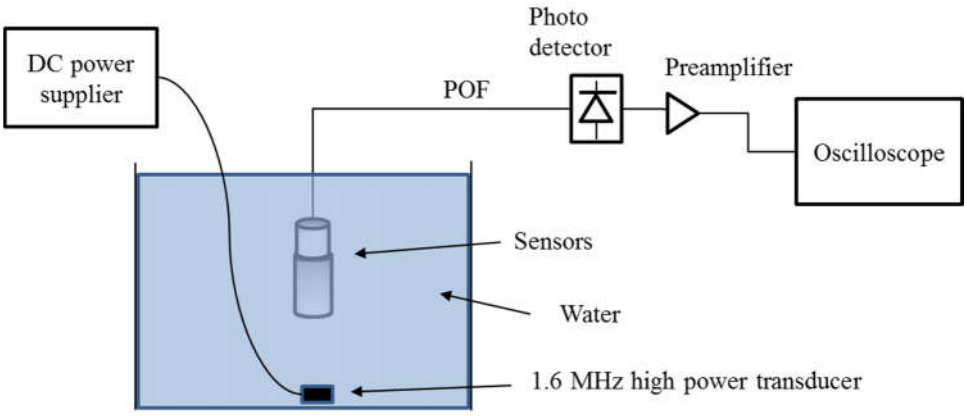

Fig. 4.22 Experimental setup of 1.6 MHz ultrasound field.

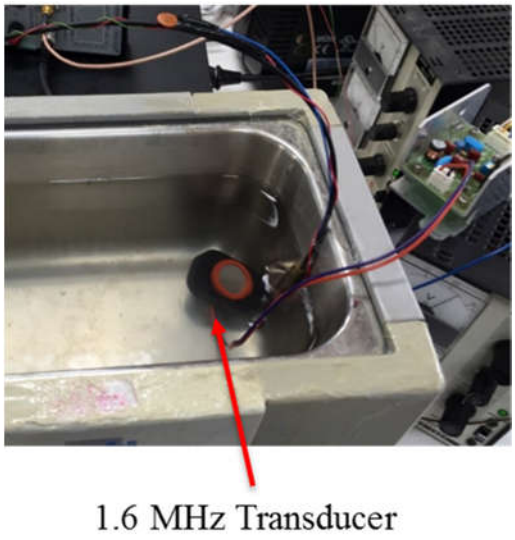

Fig. 4.23 Picture of experimental setup of 1.6 MHz ultrasound field.

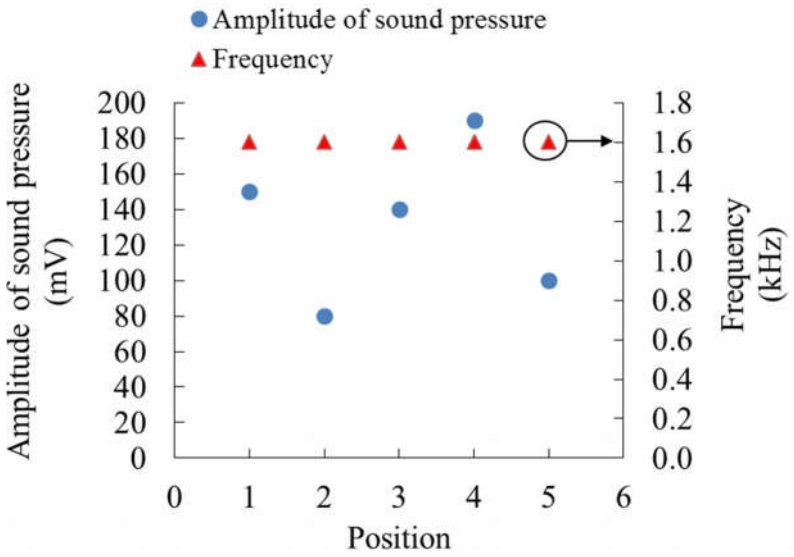

Fig. 4.24 Measured amplitude and frequency at different position by LED-PZT sensor

Moreover, we also used this sensor to measure a 1 MHz ultrasonic filed (PANAMETRICS ultrasonic computer controlled pulser/receiver, Model 5900PR, 1 MHz, available pulse energy (typical) 1, 2, 4, 8, 16, 32 μjoules;) But we cannot get any signal. It may result from the low output power of ultrasonic source.

By now we confirm the LED-PZT sensor could be used to measure different ultrasonic signal, ranging from dozens of kHz to MHz. but the sensor is not sensitive to low-power acoustic signals.

4.3 Configuration of sound intensity probe

A two-dimensional sound intensity probe shown in Fig.4.25 consists of four LED-PZT sensors. The wavelength of LEDs are 660 nm (red), 606 nm (amber), 520 nm (green) and 465 nm (blue) respectively. The distance between amber and blue sensor is 10.6 mm, which is the same with that between red and green sensor. The line between amber and

blue sensor is vertical to that between red and green sensor. We used this sensor array to measure sound pressure and phase of ultrasonic field. Finally sound intensity could be calculated from sound pressure and phase. Calculation principles is introduced in the coming "Measurement principles of sound intensity" part.

Fig. 4.26 shows the measurement system. The four different-color sensors were arranged as Fig. 4.25 and put in ultrasonic filed under water. When the probe detecting ultrasonic signals, the generated optical signals were transmitted by POFs, then measured by photo detectors (PDs) with amplifiers and finally analyzed by oscilloscope. The sound pressures of four sensors and the phase difference bet them could be read directly from oscilloscope.

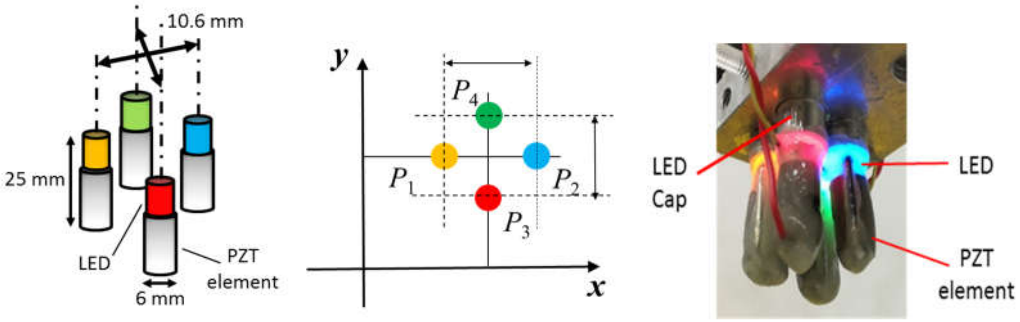

Fig. 4.25 Configuration of sound intensity probe with four LED-PZT sensors.

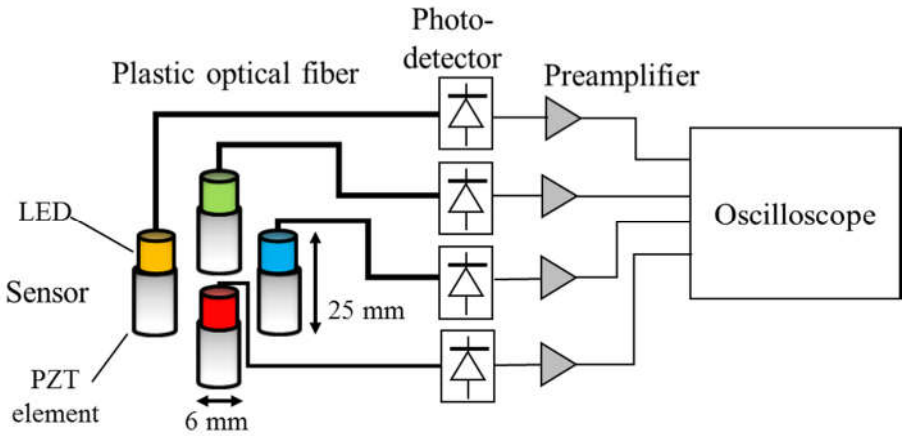

Fig. 4.26 Measurement system.

4.4 Measurement principles of sound intensity

4.4.1 Definition of sound intensity

Sound intensity, named as acoustic intensity too, is defined as the sound power per unit area. The SI unit of it is W/m2 (watt per square meter). Sound intensity $\vec{I}$ is defined by

$$\vec{I} = p\vec{v}\,, \tag{4.5}$$

where p is the sound pressure and $\vec{v}$ is the particle velocity. $\vec{I}$ and $\vec{v}$ are vectors. This equation provides instantaneous intensity. In practical measurement, normally we adopt the time-averaged sound intensity. Because the time-averaged value provides the information of net energy flow, which is known as 'active intensity'. The direction of sound intensity represent the direction of net energy flow.

4.4.2 Sound intensity's complex expression

Complex number is used to express particle velocity and sound pressure in this continuous sinusoidal sound filed. The complex particle velocity $\tilde{v}$ and sound pressure $\tilde{P}$ vector are defined as below:

$$\tilde{V} = Ve^{j\theta}\,, \tag{4.6}$$

$$\tilde{P} = Pe^{j\varphi}\,, \tag{4.7}$$

Where V, P, θ and φ are their amplitude and j is the imaginary unit. Thus reactive intensity J, which means stored energy in the field of standing wave, is expressed as imaginary part [83]:

$$J = \frac{1}{2}\mathrm{Im}\left[\tilde{P}\tilde{V}^{*}\right]. \tag{4.8}$$

Here, the complex conjugate of V is V*. The real part is active intensity *I*, which means the flowing energy in travelling wave field:

$$I = \frac{1}{2}\mathrm{Re}\left[\tilde{P}\tilde{V}^{*}\right]. \tag{4.9}$$

4.4.3 Discrete-point sound intensity measurement

In actual sound intensity measurement, sound pressure is the only parameter directly measured by sensor, while particle velocity deduced by finite difference of adjacent-point sound pressures. According to motion formula

$$j\omega\rho\tilde{V} = \mathrm{grad}\tilde{P}, \tag{4.10}$$

we have particle velocity vector $\tilde{V} = \left(\tilde{V}_x, \tilde{V}_y\right)$

$$\tilde{V}_x = \frac{\tilde{P}_2 - \tilde{P}_1}{j\omega\rho\Delta_{12}}, \tag{4.11}$$

$$\tilde{V}_y = \frac{\tilde{P}_4 - \tilde{P}_3}{j\omega\rho\Delta_{34}}. \tag{4.12}$$

$\tilde{P}_1$, $\tilde{P}_2$, $\tilde{P}_3$ and $\tilde{P}_4$ are measured complex sound pressures from four sensors as shown in Fig. 4.25.

$$\tilde{P}_i = P_i e^{j\varphi_i} \qquad (i=1, 2, 3, 4). \tag{4.13}$$

ρ *is* the density of media, while ω and Δ are the angular frequency and the distance between two sensors. P_1, P_2, P_3, P_4, φ_1, φ_2, φ_3, and φ_4 are amplitudes and phases of sound pressures. We will get these values by measurement in the following experiment part. By these measured values, finally, active components of sound intensity I_x and I_y are expressed as

$$I_x = \frac{1}{2}\mathrm{Re}\left[\tilde{P}\tilde{V}_x^{*}\right] = \frac{P_1 P_2}{2\omega\rho\Delta}\sin(\varphi_2 - \varphi_1), \tag{4.14}$$

$$I_y = \frac{1}{2}\mathrm{Re}\left[\tilde{P}\tilde{V}_y^{*}\right] = \frac{P_3 P_4}{2\omega\rho\Delta}\sin(\varphi_4 - \varphi_3)\cdot \tag{4.15}$$

While reactive components J_x and J_y are expressed as

$$J_x = \frac{1}{2}\mathrm{Im}\left[\tilde{P}\tilde{V}_x^{*}\right] = \frac{P_2^{\,2} - P_1^{\,2}}{4\omega\rho\Delta}, \tag{4.16}$$

$$J_y = \frac{1}{2}\mathrm{Im}\left[\tilde{P}\tilde{V}_y^{*}\right] = \frac{P_4^{\,2} - P_3^{\,2}}{4\omega\rho\Delta}\cdot \tag{4.17}$$

4.5 Measurement of sound intensity

4.5.1 Measurement process and error

The measurement system (Fig. 4.26) was put in this measured region (Fig. 4.14) for the sound pressure and phase. Function generator in Fig. 4.14 connected to oscilloscope in Fig. 4.26 for frequency reference. The LED-PZT sensor array measured 117 different positions in the two-dimension region. The distance between any two positions is 7.5 mm, which means 9 different positions along Y axis and 13 different positions along the X axis. Every position was measured by the sensor array to get the sound pressures and phases. According to equation (4.14)-(4.17), sound intensity could be calculated. When measurement, the line between amber and blue sensor is always parallel to x-axis, while the line between red and green sensor is always parallel to y-axis. Thus the amber LED (P1) and the blue LED (P2) sensor always measure the x-component of the intensity, while the red LED (P3) and the green LED (P4) measure y-component of the intensity. The distance between sensors was 10.6 mm, shown in Fig. 4.25, which is 18.6% of the wavelength in this 26.35-kHz ultrasonic field under water. We tried to set the distance between sensors small enough comparing with wavelength. However, if the spacing is

too small, the noise will be amplified by the according to the finite difference calculation [84].

The uniformity between four sensors should be considered. The four sensors were fixed to the mounting bracket. We can tell the distances between sensors were not perfectly like Fig. 4.25. Some sensor depart from ideal position because these hand-made sensors are not perfectly the same. The maximum distance error from ideal position is around 3 mm, which correspondingly will result in 0.3 radian phase error considering the wavelength 57 mm. Shape of measured signal was not perfectly sinusoidal sometimes, which may leads to reading error and increase the phase error to 0.6 radian.

We calculate the case when sensor has 3 mm position error. The transducer provides sinusoidal wave in ultrasonic field. We assume the center of four sensors is 0 point of sinusoidal wave, which means the sound pressure happens to be 0 in the center of four sensors. Then we assume only sensor P_2 is 3 mm away from ideal position and other sensors are in ideal positions. According to the equation of active and reactive component of sound intensity, we can calculate the active component I_x changes from -0.28 to -0.43, while I_y keeps the same. Reactive components J_x change from 0 to 0.32, while J_y keeps the same.

4.5.2 Preliminary measurement comparing with piezoelectric hydrophone

To confirm the basic performance of this new sound intensity probe, sound pressure distribution was measured first by this probe and compared with a commercialized piezoelectric hydrophone (Brüel & Kjær, 8103). The measurement results are shown in Fig. 4.27. The hydrophone scanned the field and the amplitude of sound pressure was shown in Fig. 4.27(a). We can observe the standing wave clearly along the x-direction, because the amplitude changed from trough to peak of wave periodicity along x-axis.

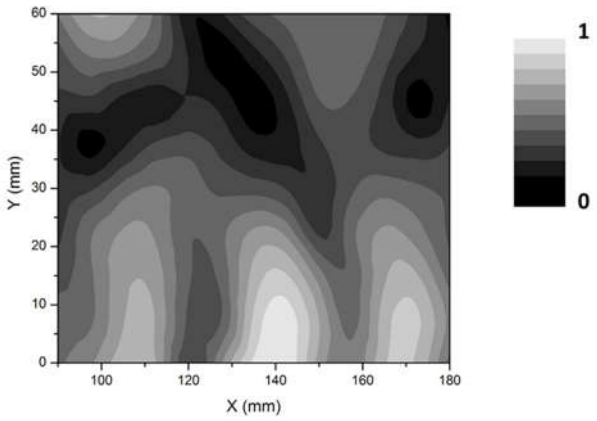

(a)

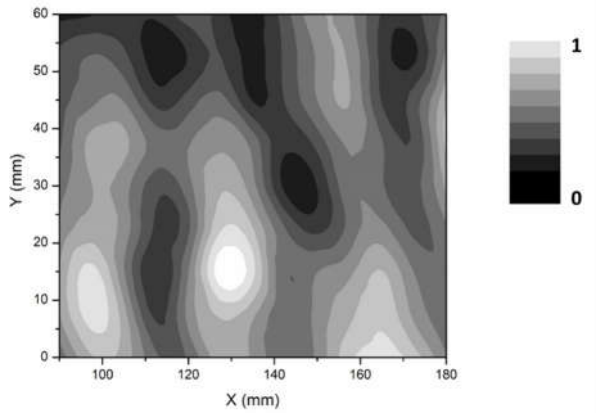

(b)

Fig. 4.27 Sound pressure distribution tested by (a) a commercialized piezoelectric hydrophone (Brüel & Kjær, 8103), and (b) sound pressure probe.

Then we used the proposed probe to scan again under almost same situation. Fig. 4.27(b) shows the average of four LED-PZT sensors in linear scale. While measurement, we tried to keep the hydrophone and the probe at the same depth in the water. Standing wave patterns are similar. The difference between two measurement results 4.27(a) and (b) may result from the instability of the ultrasonic standing wave field, which was sensitive to the water surface disturbance of the sensors insertion. Moreover, the ultrasonic field may change a little after long-time measurement for so many positions.

4.5.3 Sound intensity measurement

Figs. 4.28(a) and (b) show the measurement result of the active and reactive components of sound intensity vectors respectively by the proposed sound intensity probe when without absorbing material on the inner surfaces of water tank. Logarithmic scale is adopted for suitable length of arrows. Because there are no absorbing materials on the inner surfaces of water tank and a high reflection should be excited from the water surfaces and the walls of water tank, the field should be standing wave one. The x-components of reactive intensity changed periodically from positive to negative along the x-axis. It is typical feature of standing wave field, which agreed with sound pressure distribution in Fig. 4.27. As for the active intensity, the direction of x-components of arrows near transducer are almost positive, while the others have no such tendency.

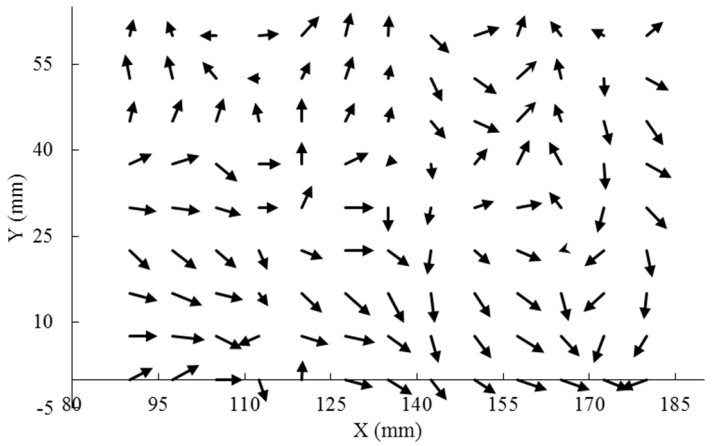

(a)

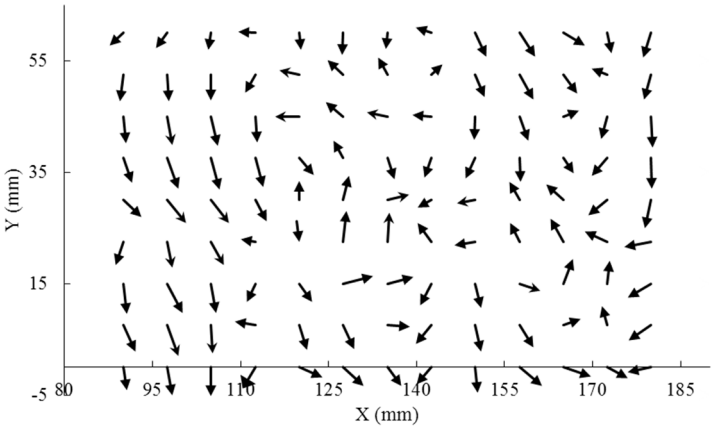

(b)

Fig. 4.28 Sound intensity distributions without absorbing material on the inner surfaces of water tank: (a) active intensity; (b) reactive intensity. Logarithmic scale are adapted for the length of arrows.

Then we fixed the absorbing materials on the inner surfaces of tank except for the water surface. In order to suppress the possibility of standing wave, we tried to reduce the parallel pair of absorbing material surfaces. The absorbing materials has corrugated surfaces and is made by sponge. The depth of rugged surface (35 mm) was 63% of the

ultrasonic wavelength (56 mm), which will also suppress the generation of standing wave. But it is clear that it is impossible to reduce reflection to zero in practice.

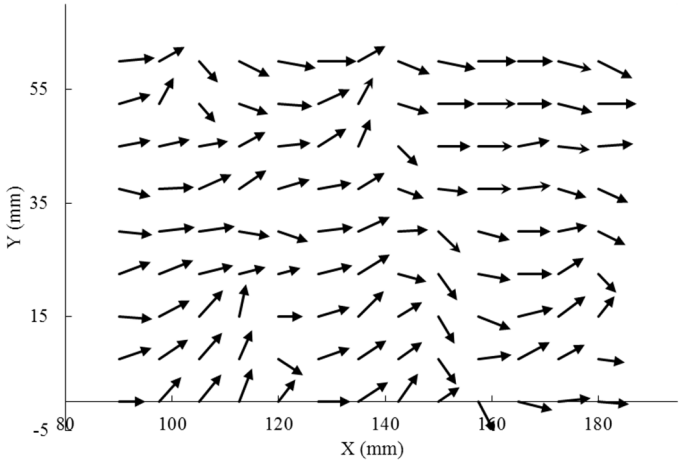

(a)

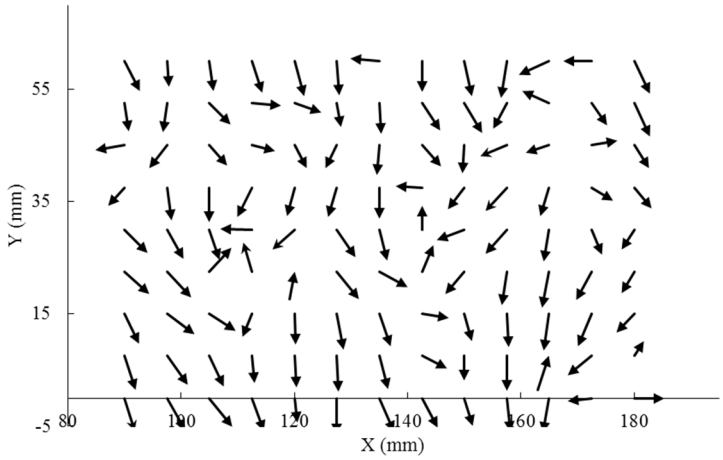

(b)

Fig. 4.29 Sound intensity distributions with absorbing material on the inner surfaces of water tank: (a) active intensity; (b) reactive intensity. Logarithmic scale are adapted for the length of arrows.

Fig. 4.29 shows the measurement results with the absorbing treatment. In Fig. 4.29(a), x-components of all positions' active intensities became positive and y-components became much smaller comparing with Fig. 4.28(a). Obviously, we could observe positive energy flux from this result. Because when adding absorbing material in tank, there were much less energy flux reflected from tank wall and the ultrasonic field was dominated by energy fluxes from transducer (travelling waves). Concerning reactive intensity in Fig. 4.29(b), x-components of arrows still alternated regularly from positive to negative along x-axis. But the periodical change of x-components become less obvious comparing with Fig. 4.28(b). It means stored energy (standing wave) reduced after adding absorbing material. Results in Fig. 4.29 met physical expectation.

For quantitative comparison between without absorber (Fig. 4.28) and with absorber (4.29), average ratio of active intensity to reactive one was calculated in Table 4.1. The ratio doubled after adding the absorber, which means the active intensity (traveling wave) increased and reactive one (standing wave) reduced. This results confirm our theoretical expectation and experimental results in Fig. 4.27 and Fig. 4.28.

Table 4.1 Ratio of active intensity to reactive intensity in the measured region.

	Average of Top 3 positions	Average of all positions
Without absorbing material in tank	0.9	1.0
With absorbing material in tank	2.1	1.8

Fig. 4.28 and Fig. 4.29 show the raw data without correction for sensitivity of every LED-PZT sensor. In the future, we will develop calibration for this intensity probe.

4.6 Final goal of this design

Actually, it is not necessary to adopt different-color LEDs in this research. Same color LEDs also work for sound intensity probe. The reason using four different-color LEDs here is, in the future research, we could adopt one fiber and wavelength division multiplexing (WDM) to transmit several sensors' signals at the same time.

Fig. 4.30 shows the final gold of this design with dense wavelength division multiplexing (DWDM). The wavelength 1, 2, 3….160 represent the signal from channel 1, 2, 3……160 respectively. These optical signals will be combined by a DWDM, transmitted by a single fiber to further place, then separated by another DWDM. Finally, when PD array detecting wavelengh1, 2, 3……160, we can know the sound pressure where channel 1, 2, 3…..160 locate correspondingly. Moreover, considering the narrow optical spectrum and optical wavelength choices requirement in this system, LED may be replaced by LD (laser diode) according to practical demands. Then LED-PZT sensor could be changed to LD-PZT sensor. Fig. 4.31 shows configuration of single LD-PZT sensor.

The idea of DWDM system comes from commercialized fiber communication system, which are already applied in telecommunications worldwide. Many networking and telecommunications equipment companies could provide such optical system, for example Huawei. The working wavelengths of the 160-channel DWDM system consist of conventional band (wavelength: 1530-1565 nm, frequency: 192.1 THz~196.0 THz) and long band (wavelength: 1565-1625 nm, frequency: 190.90 THz~186.95 THz). The

adjacent channel space is 50 GHz (namely 0.4 nm). If the channel number is not enough, we could use two or three DWDM systems at the same. The DWDM system could be replaced by CWDM (coarse wavelength division multiplexer) system, if the system has less channel number demands. Its adjacent channel space is 20 nm and it has much less technical requirements and cost comparing with DWDM system.

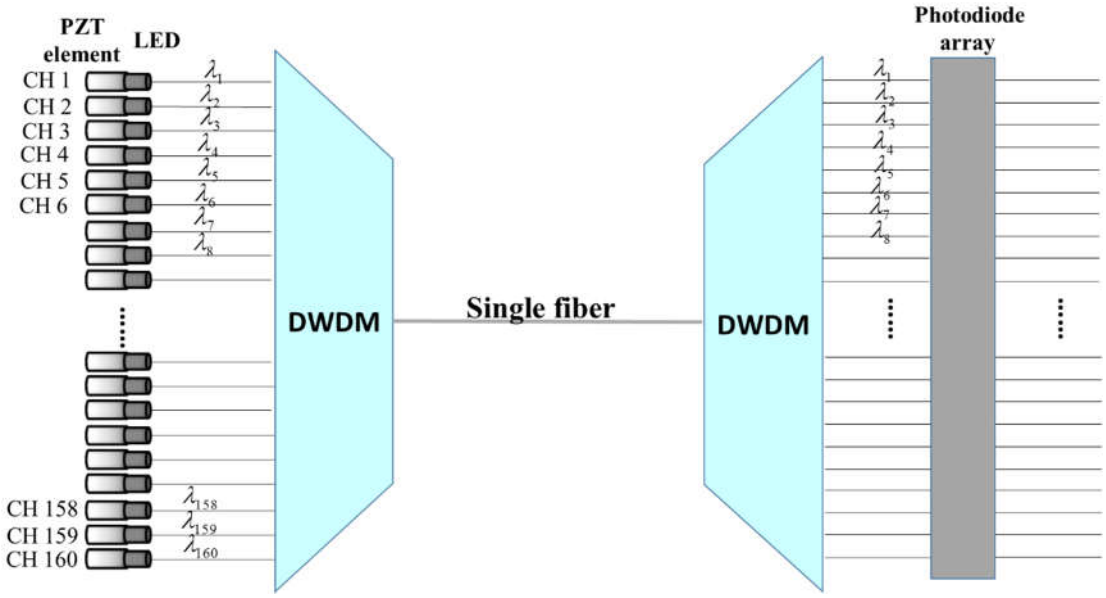

Fig. 4.30 Final goal of this design with DWDM

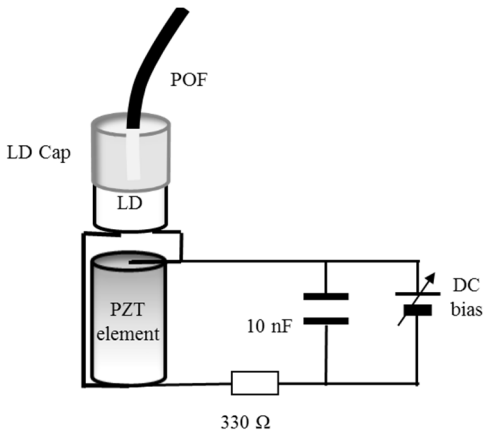

Fig. 4.31 Configuration of single LD-PZT sensor.

This design can replace the metal wire bundle of conventional detector array by single fiber and make the system lighter, smaller and longer transmitting distance.

4.7 Conclusions

A novel acoustic detector consisting of LED and PZT element was proposed and called LED-PZT sensor. Its characteristics were invested experimentally in 26 kHz, 38 kHz and 1.6 MHz ultrasound field underwater and its effectiveness was demonstrated. Then a two-dimensional sound intensity probe, consisting of four LED-PZT sensors, was fabricated. As preliminary testing, sound pressure distribution was measured by the probe in a 26 kHz ultrasonic field underwater and comparing with a commercialized conventional hydrophone. Then sound intensity measurement was conducted and intensity vector maps were acquired in the 26 kHz ultrasonic field underwater with and without absorber. The results show the effectiveness of this novel probe. This new technique make handling of the cables easy between the electronic equipment for signal processing and the sensor head by adopting optical fiber. It is lighter (only 33% of conventional hydrophone weight), smaller and longer transmitting distance comparing with conventional acoustic detector.

In the future, firstly, this LED-PZT sensor could be upgraded to LD-PZ. This two-dimensional measurement could be upgraded to three-dimensional measurements by adopting wavelength division multiplex (WDM) to reduce multi-fiber to single fiber for long-distance transmitting. 160-channel may work at the same time by a dense wavelength division multiplex (DWDM. It will make the measurement system more compact, and could be applied in medicine and industry. Secondly, calibration method

will be established for more precise measurement. For MHz high power ultrasonic application, which become common in industrial and medical fields, the sensor should be miniaturized by adopting smaller piezoelectric element and tip LED.

Chapter 5

Conclusions and future work

5.1 Summary

This thesis proposes a compact photoacoustic system for materials evaluation, especially for photoacoustic contrast agent in biomedicine. Moreover, a novel acoustics detector is designed for photoacoustics and other related acoustic detection. This chapter specifies the conclusions that can be drawn from this thesis into photoacoustic spectroscopy and acoustics detection, which relate to the following chapters.

In Chapter 1: “Introduction”, conventional medical imaging techniques were introduced. Basing on their limitations, photoacoustic method was proposed. Then the fundamentals, history and development of photoacoustics were introduced. Because current photoacoustic implementations were normally large and expensive, we proposed our objective to develop a portable and cheap photoacoustic system for non-destructive material evaluation. Moreover, we proposed a novel acoustic detector which could be applied in photoacoustics and other acoustics applications. The organization of this thesis was introduced too.

In Chapter 2: “Compact photoacoustic system for sensitivity evaluation of materials”, a portable photoacoustic system was proposed for non-destructive materials evaluation with dual laser diodes working with modulated continuous waves and a MEMS microphone at low-frequency (kHz) region. Fundamentals and design of PA system are described. Then the characteristics of PA system and its key component PA cell was experimentally investigated by testing black ink, dye ink and its mixture solution samples to confirm its effectiveness and high sensitivity. Wood was also measured as sample. This system could distinguish very small absorption coefficient difference of water between 0.004 at 660 nm and 0.01 at 785 nm. It also tell 10 mg/dl concentration difference of black ink solution.

In Chapter 3: “Photoacoustic contrast agent evaluation by proposed compact photoacoustic system”, we used the photoacoustic system introduced in chapter 2 to evaluate photoacoustic contrast agents, including ICG solution, TO-001, TO-002 and TO-003 solution. This non-destructive testing system is sensitive and can distinguish 2.5 μmol/L concentration difference of ICG solution at 785 nm. We have also developed a new method to test sample with small volume by this PA. We confirm this PA system is suitable for liquid, solid and powder testing. Further characteristics of PA system were demonstrated by these contrast agent evaluation, for example how noises affecting photoacoustic measurements. A strange phenomenon with high concentration solution measurement was described too.

In Chapter 4: “Sound intensity measurement for ultrasound under water using light emitting diodes and piezoelectric elements”, a novel acoustic detector, called LED-PZT sensor, was proposed. This sensor consists of light emitting diode (LED), piezoelectric (PZT) element and a plastic optical fiber (POF). Its characteristics was experimentally

invested in 26 kHz, 38 kHz and 1.6 MHz ultrasound field to demonstrate its effectiveness. Then four LED-PZT sensors were combined to fabricate a novel two dimensional sound intensity probe. Sound pressure distribution in a 26 kHz ultrasonic field was measured first by this probe underwater and compared with a conventional hydrophone. Similar standing wave patterns were observed by both methods and its preliminary confirmation was done. Then sound intensity distribution was measured and plotted for the 26 kHz ultrasonic field by the probe underwater with and without absorber. The results meet our theoretical expectation. This novel acoustic detector can work as conventional one and it is lighter (33% of conventional hydrophone weight), smaller and longer transmitting distance.

5.2 Future work

Both photoacoustic and LED-PZT sensor are interesting and promising research fields. Although the newly proposed photoacoustic system and LED-PZT sensor shows great effectiveness, there are surely still some remaining questions and are worthwhile to investigate in future.

For more precise measurement of PA system, a mass flow controller with needle shape (for example: MKS Instruments, Multi Gas Controller 647B) could be connected to PA cell to provide constant flow of N2 gas into the cell and guarantee stable conditions inside the cell. Then ink solutions and contrast agents could be measured again and higher evaluation sensitivity should be achieved.

Temperature and humidity are another two key factors to affect PA system. We could add a temperature and humidity sensor (for example: Sensirion SHT21, 3 mm x 3

mm x 1.1 mm), for example just beside microphone, to simultaneously monitor the temperature and relative humidity inside PA cell. Then we could experimentally investigate how temperature and humidity affect photoacoustic signals. By temperature and humidity controller, higher evaluation sensitivity of PA system could be expected.

We already confirm this PA system could evaluate liquid non-destructively. It could be enhanced to evaluate solid and gas by adopting two piece of glass to two ends of PA cell. The glass should have low absorption coefficient at working wavelengths. As for solid measurement, the measured solid could be put just on the glass. By this way, the PA signals come from the optical absorption of target solid and are amplified by the PA cell. The characteristics of target solid could be confirmed by PA signals, for example absorption of target. Gas could be measured by this same system if it is contained inside the PA cell.

Current PA system adopts a MEMS microphone working at low-frequency (kHz) region. A MHz PA system could be developed by adopting laser diodes modulated by MHz function generator and MHz transducer. MHz is common working frequency in biomedicine and PAT, which is PA contrast agent will be applied in. We could compare the measurement results from kHz and MHz photoacoustic system to get comprehensive understanding of contrast agents and PA system. In principle, the measurement results should be the same but may have some new characteristics.

Another potential application for this portable PA system is handheld and noninvasive medical equipment. It could measure chromophore concentration in human blood and tissue noninvasively and immediately, for example hemoglobin and glucose. Currently, most of medical PA researches focus on imaging application, but these implementations are large and expensive. This compact and cheap system could

supplement the demand of daily health diagnosis (home health care), or work for performance evaluation and control of exercise intensity in sport training. In this application, temperature and humidity monitor is necessary for this system. Because the human tissues will change the temperature and humidity obviously. More functions and specifications should be considered according to the specific demands.

As for the LED-PZT sensor, it could be upgraded to LD-PZT sensor by replacing LED by LD (laser diode) using the same sensor configuration. LD-PZT sensor has more optical wavelength choices, narrower optical spectrum and its optical signal could be transmitted by fiber with less transmitting loss. Then 160-channel optical signals with different wavelengths from 160 LD-PZT sensors are combined by a DWDM (Dense Wavelength Division Multiplexing) and transmitted by single fiber to remote area for signal processing and control. Finally we could know the sound pressure distribution where the 160 different sensors locate, because specific optical wavelength represent the corresponding sensor. Actually, the system could be changed again by replacing DWDM by several CWDMs (Coarse Wavelength Division Multiplexing) and replacing single fiber by several fibers. In this design, the system has less requirements with LD and wavelength control.

References

[1] Upputuri, Paul Kumar, et al. "Recent developments in vascular imaging techniques in tissue engineering and regenerative medicine." BioMed research international 2015 (2015).

[2] Wang LV, Wu H-i. Biomedical optics: principles and imaging: John Wiley & Sons; 2012.

[3] Wang, Lihong V., and Song Hu. "Photoacoustic tomography: in vivo imaging from organelles to organs." Science 335.6075 (2012): 1458-1462

[4] Xu, Minghua, and Lihong V. Wang. "Photoacoustic imaging in biomedicine." Review of scientific instruments 77.4 (2006): 041101.

[5] Lipson, Ariel, Stephen G. Lipson, and Henry Lipson. Optical physics. Cambridge University Press, 2010. p. 405

[6] Wang LV. Photoacoustic imaging and spectroscopy: CRC press; 2009.

[7] Bell, Alexander Graham. "The production of sound by radiant energy." Science 2.48 (1881): 242-253.

[8] Vargas, H., and L. C. M. Miranda. "Photoacoustic and related photothermal techniques." Physics Reports 161.2 (1988): 43-101.

[9] Sigrist, M. W. "Trace gas monitoring by laser-photoacoustic spectroscopy." Infrared Physics & Technology 36.1 (1995): 415-425.

[10] Oliver, N. S., et al. "Glucose sensors: a review of current and emerging technology." Diabetic Medicine 26.3 (2009): 197-210.

[11] Wang, Lihong V. "Multiscale photoacoustic microscopy and computed tomography." Nature photonics 3.9 (2009): 503-509.

[12] Ntziachristos, Vasilis, et al. "Looking and listening to light: the evolution of whole-body photonic imaging." Nature biotechnology 23.3 (2005): 313-320.

[13] Maslov, Konstantin, and Lihong V. Wang. "Photoacoustic imaging of biological tissue with intensity-modulated continuous-wave laser." Journal of biomedical optics 13.2 (2008): 024006-024006.

[14] Wang, Lihong V. "Prospects of photoacoustic tomography." Medical physics 35.12 (2008): 5758-5767.

[15] Wang, Xueding, et al. "Noninvasive laser-induced photoacoustic tomography for structural and functional in vivo imaging of the brain." Nature biotechnology 21.7 (2003): 803-806.

[16] Wang, Xueding, et al. "Noninvasive imaging of hemoglobin concentration and oxygenation in the rat brain using high-resolution photoacoustic tomography." Journal of biomedical optics 11.2 (2006): 024015-024015.

[17] Cox, Ben, et al. "Quantitative spectroscopic photoacoustic imaging: a review." Journal of biomedical optics 17.6 (2012): 0612021-06120222.

[18] Zhang, Hao F., et al. "Imaging of hemoglobin oxygen saturation variations in single vessels in vivo using photoacoustic microscopy." Applied physics letters 90.5 (2007): 053901.

[19] Hu, Song, Konstantin Maslov, and Lihong V. Wang. "Second-generation optical-resolution photoacoustic microscopy with improved sensitivity and speed." Optics letters 36.7 (2011): 1134-1136.

[20] Zhang, Hao F., et al. "Functional photoacoustic microscopy for high-resolution and noninvasive in vivo imaging." Nature biotechnology 24.7 (2006): 848-851.

[21] Xu, Minghua, and Lihong V. Wang. "Universal back-projection algorithm for photoacoustic computed tomography." Physical Review E 71.1 (2005): 016706.

[22] Yang, Joon-Mo, et al. "Photoacoustic endoscopy." Optics letters 34.10 (2009): 1591-1593.

[23] Niederhauser, Joël J., et al. "Combined ultrasound and optoacoustic system for real-time high-contrast vascular imaging in vivo." IEEE transactions on medical imaging 24.4 (2005): 436-440.

[24] Wang, Yu, et al. "In vivo three-dimensional photoacoustic imaging based on a clinical matrix array ultrasound probe." Journal of Biomedical Optics 17.6 (2012): 0612081-0612085.

[25] Li, Changhui, and Lihong V. Wang. "Photoacoustic tomography and sensing in biomedicine." Physics in medicine and biology 54.19 (2009): R59.

[26] Hodgkinson, Jane, and Ralph P. Tatam. "Optical gas sensing: a review." Measurement Science and Technology 24.1 (2012): 012004.

[27] Moosmüller, H., R. K. Chakrabarty, and W. P. Arnott. "Aerosol light absorption and its measurement: A review." Journal of Quantitative Spectroscopy and Radiative Transfer 110.11 (2009): 844-878.

[28] Arnott, W. Patrick, et al. "Photoacoustic spectrometer for measuring light absorption by aerosol: instrument description." Atmospheric Environment 33.17 (1999): 2845-2852.

[29] Li, Jingsong, Weidong Chen, and Benli Yu. "Recent progress on infrared photoacoustic spectroscopy techniques." Applied Spectroscopy Reviews 46.6 (2011): 440-471.

[30] Miklós, András, Peter Hess, and Zoltán Bozóki. "Application of acoustic resonators in photoacoustic trace gas analysis and metrology." Review of scientific instruments 72.4 (2001): 1937-1955.

[31] Bernegger, Stefan, and M. W. Sigrist. "CO-laser photoacoustic spectroscopy of gases and vapours for trace gas analysis." Infrared Physics 30.5 (1990): 375-429.

[32] Kosterev, Anatoliy A., et al. "Quartz-enhanced photoacoustic spectroscopy." Optics letters 27.21 (2002): 1902-1904.

[33] Dong, Lei, et al. "QEPAS spectrophones: design, optimization, and performance." Applied Physics B: Lasers and Optics 100.3 (2010): 627-635.

[34] Schmid, Thomas. "Photoacoustic spectroscopy for process analysis." Analytical and bioanalytical chemistry 384.5 (2006): 1071-1086.

[35] Braslavsky, Silvia E., and George E. Heibel. "Time-resolved photothermal and photoacoustic methods applied to photoinduced processes in solution." Chemical reviews 92.6 (1992): 1381-1410.

[36] Laufer, Jan, et al. "Quantitative spatially resolved measurement of tissue chromophore concentrations using photoacoustic spectroscopy: application to the measurement of blood oxygenation and haemoglobin concentration." Physics in medicine and biology 52.1 (2006): 141.

[37] Laarhoven, Lucas JJ, Peter Mulder, and Danial DM Wayner. "Determination of bond dissociation enthalpies in solution by photoacoustic calorimetry." Accounts of chemical research 32.4 (1999): 342-349.

[38] Pleitez, Miguel A., et al. "In vivo noninvasive monitoring of glucose concentration in human epidermis by mid-infrared pulsed photoacoustic spectroscopy." Analytical chemistry 85.2 (2012): 1013-1020.

[39] Galanzha, Ekaterina I., and Vladimir P. Zharov. "Photoacoustic flow cytometry." Methods 57.3 (2012): 280-296.

[40] Zharov, Vladimir P., et al. "In vivo photoacoustic flow cytometry for monitoring of circulating single cancer cells and contrast agents." Optics letters 31.24 (2006): 3623-3625.

[41] Rai, A. K., and J. P. Singh. "Perspective of photoacoustic spectroscopy in disease diagnosis of plants: a review." Instrumentation Science & Technology 31.4 (2003): 323-342.

[42] Herbert, Stephen K., David C. Fork, and Shmuel Malkin. "Photoacoustic measurements in vivo of energy storage by cyclic electron flow in algae and higher plants." Plant Physiology 94.3 (1990): 926-934.

[43] Gensch, Thomas, and Cristiano Viappiani. "Time-resolved photothermal methods: accessing time-resolved thermodynamics of photoinduced processes in chemistry and biology." Photochemical & Photobiological Sciences 2.7 (2003): 699-721.

[44] Hung, Rebecca R., and Joseph J. Grabowski. "A precise determination of the triplet energy of carbon (C60) by photoacoustic calorimetry." The Journal of Physical Chemistry 95.16 (1991): 6073-6075.

[45] Lai, H. M., and K. Young. "Theory of the pulsed optoacoustic technique." The Journal of the Acoustical Society of America 72.6 (1982): 2000-2007.

[46] Fang, Hui, Konstantin Maslov, and Lihong V. Wang. "Photoacoustic Doppler effect from flowing small light-absorbing particles." Physical Review Letters 99.18 (2007): 184501.

[47] Fang, Hui, Konstantin Maslov, and Lihong V. Wang. "Photoacoustic Doppler flow measurement in optically scattering media." Applied Physics Letters 91.26 (2007): 264103.

[48] Haisch, Christoph. "Photoacoustic spectroscopy for analytical measurements." Measurement Science and Technology 23.1 (2011): 012001.

[49] Ma, Cheng, et al: "Time-reversed adapted-perturbation (TRAP) optical focusing onto dynamic objects inside scattering media." Nature photonics 8.12 (2014) 931.

[50] Yang, Joon-Mo, et al: "Simultaneous functional photoacoustic and ultrasonic endoscopy of internal organs in vivo." Nature medicine 18.8 (2012) 1297.

[51] Favazza, Christopher P., et al: "In vivo photoacoustic microscopy of human cutaneous microvasculature and a nevus." Journal of biomedical optics 16.1 (2011) 016015.

[52] Lewin, P. A. "Miniature piezoelectric polymer ultrasonic hydrophone probes." Ultrasonics 19.5 (1981): 213-216.

[53] Platte, M. "A polyvinylidene fluoride needle hydrophone for ultrasonic applications." Ultrasonics 23.3 (1985): 113-118.

[54] Spillman Jr, W. B., and D. H. McMahon. "Schlieren multimode fiber-optic hydrophone." Applied Physics Letters 37.2 (1980): 145-147.

[55] Spillman, W. B. "Multimode fiber-optic hydrophone based on a schlieren technique." Applied Optics 20.3 (1981): 465-470.

[56] Staudenraus, Joachim, and Wolfgang Eisenmenger. "Fibre-optic probe hydrophone for ultrasonic and shock-wave measurements in water." Ultrasonics 31.4 (1993): 267-273.

[57] Zhou, Yufeng, et al. "Measurement of high intensity focused ultrasound fields by a fiber optic probe hydrophone." The Journal of the Acoustical Society of America 120.2 (2006): 676-685.

[58] Koch, Ch. "Coated fiber-optic hydrophone for ultrasonic measurement." Ultrasonics 34.6 (1996): 687-689.

[59] Beard, P. C., and T. N. Mills. "Miniature optical fibre ultrasonic hydrophone using a Fabry-Perot polymer film interferometer." Electronics Letters 33.9 (1997): 801-803.

[60] *for example,* K Yamomoto, Optical visualization of acoustic fields: the schlieren technique, the Fresnel method and the photoelastic method applied to ultrasonic transducers, in: Nakamura, Kentaro, ed. Ultrasonic transducers: Materials and design for sensors, actuators and medical applications. Elsevier, 2012, pp. 314-327. Chap. 10.

[61] Neumann, Thorsten, and Helmut Ermert. "Schlieren visualization of ultrasonic wave fields with high spatial resolution." Ultrasonics 44 (2006): e1561-e1566.

[62] Ohno, Masahiro. "Observation of Ultrasonic Fields Transmitted through Bovine Cortical or Cancellous Bones by the Schlieren Method." Japanese Journal of Applied Physics 48.7S (2009): 07GC10.

[63] *for example,* F. Jacobsen, Sound intensity, in: Dunn, F., et al. Springer handbook of acoustics. Springer, 2015, pp. 1093-1112. Chap. 25.

[64] Hutt, Daniel L., Paul C. Hines, and Andrew AJ Hamilton. "Measurements of underwater sound intensity vector." OCEANS'99 MTS/IEEE. Riding the Crest into the 21st Century. Vol. 2. IEEE, 1999.

[65] Bastyr, Kevin J., Gerald C. Lauchle, and James A. McConnell. "Development of a velocity gradient underwater acoustic intensity sensor." The Journal of the Acoustical Society of America 106.6 (1999): 3178-3188.

[66] Gloza, I. "Experimental investigation of underwater noise produced by ships by mean of sound intensity method." Acta Physica Polonica A 118.1 (2010): 58-61.

[67] Nakamura, K., and T. Sugimoto. "Measurements of ultrasonic field using a piezoelectric-ceramics and a light emitting diode." Trans IEICE 86.12 (2003): 1331-1336.

[68] Nakamura, Kentaro, and Tsuneyoshi Sugimoto. "8F-5 A Visualization Tool for High Intensity Focused Ultrasonic Field Using LEDs and Piezo-Elements." Ultrasonics Symposium, 2007. IEEE. IEEE, 2007.

[69] Nakamura, K., H. Ogura, and T. Sugimoto. "Direct visualization of high-intensity focused ultrasonic field using light-emitting diodes and piezoelectric elements." Acoustical Imaging (2009): 309-316.

[70] Rosencwaig, Allan, and Allen Gersho. "Theory of the photoacoustic effect with solids." Journal of Applied Physics 47.1 (1976): 64-69.

[71] Tam, Andrew C. "Applications of photoacoustic sensing techniques." Reviews of Modern Physics 58.2 (1986): 381.

[72] Lambert, Johann Heinrich. Photometria sive de mensura et gradibus luminis, colorum et umbrae. Klett, 1760.

[73] Pierce, Allan D. Acoustics: an introduction to its physical principles and applications.

Vol. 678. New York: McGraw-Hill, 1981.

[74] Hu, Song, Konstantin Maslov, and Lihong V. Wang. "Second-generation optical-resolution photoacoustic microscopy with improved sensitivity and speed." Optics letters 36.7 (2011): 1134-1136.

[75] Favazza, Christopher P., et al. "In vivo photoacoustic microscopy of human cutaneous microvasculature and a nevus." Journal of biomedical optics 16.1 (2011): 016015-016015.

[76] Ku, Geng, et al. "Copper sulfide nanoparticles as a new class of photoacoustic contrast agent for deep tissue imaging at 1064 nm." Acs Nano 6.8 (2012): 7489-7496.

[77] Li, Changhui, and Lihong V. Wang. "Photoacoustic tomography and sensing in biomedicine." Physics in medicine and biology 54.19 (2009): R59.

[78] De La Zerda, Adam, et al. "Carbon nanotubes as photoacoustic molecular imaging agents in living mice." Nature nanotechnology 3.9 (2008): 557-562.

[79] Eghtedari, Mohammad, et al. "High sensitivity of in vivo detection of gold nanorods using a laser optoacoustic imaging system." Nano letters 7.7 (2007): 1914-1918.

[80] Filonov, Grigory S., et al. "Deep‐Tissue Photoacoustic Tomography of a Genetically Encoded Near‐Infrared Fluorescent Probe." Angewandte Chemie International Edition 51.6 (2012): 1448-1451.

[81] Herzog, Eva, et al. "Optical imaging of cancer heterogeneity with multispectral optoacoustic tomography." Radiology 263.2 (2012): 461-468.

[82] Wang, Lihong V., and Hsin-I. Wu. Biomedical optics: principles and imaging. John Wiley & Sons, 2012.

[83] M.J. Crocker, J.P. Arenas, Fundamentals of the direct measurement of sound intensity and practical applications, Acoust. Phys. 49 (2003) 163‐175.

[84] L. Lapidus, G.F. Pinder, Numerical solution of partial differential equations in science and engineering, John Wiley & Sons, 2011.

Related publications

Journal papers

1. Xi Zeng, Yosuke Mizuno, Kentaro Nakamura, Sound intensity probe for ultrasonic field in water using light emitting diodes and piezoelectric elements, Jpn. J. Appl. Phys., (Accepted for publication)
2. Xi Zeng, Yosuke Mizuno, Kentaro Nakamura, photoacoustic measurement system for sensitivity estimating of material, Acoustical science and technology (Accepted for publication)

Domestic conference proceedings

1. Xi Zeng, Marie Tabaru, Kentaro Nakamura, Low-frequency photoacoustic measurement system by using dual laser diodes working with modulated continuous wave, 2016 Spring Meeting, Acoustical Society of Japan, 2-7-5.